Photocatalytic CO_2 reduction

Siyuan Fang[1], Motiar Rahaman[2], Jaya Bharti[3], Erwin Reisner[2], Marc Robert[3,4], Geoffrey A. Ozin[5], Yun Hang Hu[1]*

[1]Department of Materials Science and Engineering, Michigan Technological University, Houghton, Michigan, United States

[2]Yusuf Hamied Department of Chemistry, University of Cambridge, Cambridge, United Kingdom

[3]Laboratoire d'Electrochimie Moléculaire, Université Paris Cité, CNRS, Paris, France

[4]Institut Universitaire de France, Paris, France

[5]Department of Chemistry, University of Toronto, Toronto, Canada

[*]email: yunhangh@mtu.edu

Abstract

Using sunlight to power CO_2 conversion into value-added chemicals and fuels is a promising technology to use anthropogenic CO_2 emissions to alleviate our dependence on fossil fuels. In this Primer, we provide a holistic step-by-step guide for the experimentation of photocatalytic CO_2 reduction, including catalyst synthesis and characterization, reactor construction, photocatalytic testing, and mechanism exploration. We compare and analyse the state-of-the-art results with different photocatalysts and discuss possible reaction mechanisms. Furthermore, important considerations regarding practical application of photocatalytic CO_2 reduction are highlighted and strategies to enhance energy conversion efficiency and product selectivity are summarized. This Primer also reveals current issues of reproducibility, standardizes data reporting, and proposes a unified operation condition. Finally, future directions are outlined in terms of experiments, calculations, big-data development, and practical application.

[H1] Introduction

The content of carbon dioxide (CO_2) in the atmosphere has significantly increased to 420 ppm from approximately 280 ppm in the early 1800s [1,2]. This is mainly due to the extensive exploitation of fossil fuels, with the current global fossil CO_2 emissions having reached 36.3 gigatons per year and continuing to grow[2]. This linear fossil-to-CO_2 economy model is causing global warming, sea level rise, ocean acidification, extreme weather, species extinction and food shortage[3,4]. The development of efficient decarbonization technologies to capture, store and utilize CO_2 could mitigate these issues.

CO_2 capture and geological sequestration require large energy consumption, but the utilization of CO_2 as a feedstock for producing value-added chemicals and fuels is an attractive long-term proposition to complete the carbon cycle[5-8]. For example, CO_2 can be converted to carbon monoxide (CO), formic acid (HCOOH), formaldehyde (HCHO), methanol (CH_3OH), methane (CH_4), as well as multi-carbon chemicals such as oxalic acid ($H_2C_2O_4$), acetic acid (CH_3COOH), acetaldehyde (CH_3CHO), ethanol (CH_3CH_2OH), ethylene (C_2H_4), and ethane (C_2H_6) via a series of reduction reactions. As summarized in **Table 1**, these products have high market prices, ranging from 0.1 to 2.0 US \$ kg^{-1}, with broad applications in chemical production, clean fuels, metallurgy, solvation, disinfection, bleaching, food and beverage, leather and textile industry, and cryogenic refrigeration system[9].

Many approaches have been explored for CO_2 conversion to date, including thermal catalysis, electrocatalysis, and photocatalysis. Thermal catalysis generally shows high efficiencies for CO_2 reduction, but harsh conditions with high temperatures and high pressures are often required, causing considerable energy cost and safety issues[10,11]. Electrocatalysis is performed under an external electric field, in which there is a trade-off between the catalytic activity and selectivity, owing to the excessive overpotential[12,13]. In contrast, photocatalysis relies on solar energy for CO_2 reduction, demonstrating several advantages such as mild operation condition, small energy consumption and ready availability[14,15]. Therefore, photocatalytic CO_2 reduction has attracted enormous research interests since the pioneering work to drive CO_2 reduction into HCHO and CH_3OH[16] by illuminating the aqueous suspensions of various semiconductor powders including TiO_2, ZnO, CdS, GaP, and SiC.

Photocatalytic CO_2 reduction approaches can be categorized into heterogenous and homogenous processes. Heterogenous processes are typically based on semiconductor or plasmonic metal solid photocatalysts. As illustrated in **Fig. 1a**, photocatalytic CO_2 reduction over a semiconductor photocatalyst undergoes at least three mechanistic steps[5,17]. Firstly, light with photon energy equal to or greater than the semiconductor energy band gap is absorbed, exciting the electrons from the valence band maximum (VBM) to the conduction band minimum (CBM)**,** while leaving holes at the VBM. Next, the photo-generated electrons and holes transfer to the catalyst surface (through cocatalyst if applicable). Finally, adsorbed CO_2 is

reduced by photo-generated electrons and the adsorbed reductant is oxidized by photo-generated holes. Ideally, CO_2 reduction is accompanied by water oxidation or some other value-added oxidations. Moreover, such a process must satisfy two thermodynamic requirements. Namely, the redox potential of reduction half-reaction must be more positive than the CBM, and the redox potential of oxidation half-reaction must be more negative than the VBM. Common CO_2 reduction half-reactions and corresponding apparent standard redox potentials (at pH = 7) are summarized in **Table 1**. In addition, from the perspective of reaction kinetics, there must be catalytic sites where CO_2 activation takes place.

It is effective to fabricate heterostructure catalysts with favourable band alignment to enable broad spectral responses and efficient charge separation. According to charge transfer directions, heterostructure catalysts are divided into p-n junction and Z-scheme[18-22]. In a p-n junction (**Fig. 1b**), photo-generated electrons are injected to the component with more positive CB position, while photo-generated holes migrate to the component with more negative VB position. Differently, in a Z-scheme architecture (**Fig. 1c**), photo-generated electrons in the component with more positive CB position are injected into the VB of another component with a more negative position either directly or indirectly with conductive intermediate or reversible redox shuttle.

Furthermore, heterogenous photocatalytic CO_2 reduction can be carried out over metal catalysts such as gold, silver, copper and bismuth, which mainly owes to the localized surface plasmon resonance effect (**Fig. 1d**)[23-26]. Namely, after collective oscillation of surface electrons is excited by incident photons at the resonant frequency, local heat is generated and hot charge carriers are formed through intra-band s-to-s or inter-band d-to-s transitions under the strong surface electric field[27]. Both the local heat and hot charge carriers can contribute to CO_2 reduction[26,28].

The mechanistic steps of homogenous photocatalytic CO_2 reduction are like those over semiconductor catalysts, though with the participation of photosensitizer and molecular catalyst instead. As shown in **Fig. 1e**, the photosensitizer is excited upon light absorption and then reductively quenched by the reductant, forming a reduced photosensitizer molecule[29]. The reduced photosensitizer injects electrons to the molecular catalyst, transforming it from the oxidized state to reduced state. The reduced molecular catalyst then donates electrons to CO_2 to realize its reduction. The alternative mechanism of oxidative quenching is less common in photocatalytic CO_2 reduction processes[30]. Furthermore, there are hybrid processes in which a molecular catalyst is attached to a heterogeneous semiconductor via covalent or non-covalent interactions[31]. In this case, the semiconductor is responsible for charge carrier excitation while the molecular catalyst provides active sites for CO_2 reduction (performing as a cocatalyst).

This Primer focuses on photocatalytic approaches to convert CO_2 into value-added chemicals and fuels. A general method for conducting photocatalytic CO_2 reduction

experiments is summarized in terms of catalyst synthesis, catalyst characterization, experimental setup, photocatalytic test and mechanism exploration. Afterward, a state-of-the-art overview on important metrics and possible mechanisms of photocatalytic CO_2 reduction is provided, followed by an in-depth analysis of the considerations for its practical application. This Primer also reveals the factors hindering reproducibility and elucidates the data reporting requirements and standard operation condition. Finally, the main limitations and corresponding optimization strategies are discussed, and future directions are outlined.

[H1] Experimentation

A general overview for conducting photocatalytic CO_2 reduction experiments is presented in **Fig. 2**, including five steps, namely, catalyst synthesis, catalyst characterization, assembly of the photocatalytic reactor, performing photocatalytic tests and exploring reaction mechanisms.

[H2] Catalyst synthesis

The photocatalytic system applied for CO_2 reduction generally consists of a light absorber and cocatalyst. In many cases, the light absorber and cocatalyst are synthesized independently and then combined to give a functional assembly. In heterogeneous photocatalytic systems, light absorbers are mainly metals[23,24,52] and alloys[43] organic frameworks such as metal organic frameworks (MOFs)[53-56] and covalent organic frameworks (COFs)[36,57,58] or inorganic semiconductors. Typical inorganic semiconductors include metal oxides[32-35], metal sulfides[36-39], metal oxyhalides[40-42], layered double hydroxides[43,44] and graphene-like 2D materials (such as g-C_3N_4, graphene oxide)[20,41,45-51]. Most of the inorganic semiconductors are commercially available. However, inorganic semiconductors with various crystal phases, morphologies, particle sizes, and defects/vacancies can be synthesized to provide more insights into the structure-property-performance relationship and acquire more flexibility to achieve the optimal photocatalytic performance, Synthesis of the inorganic semiconductors include calcination, hydro/solvo-thermal reaction, co-precipitation, chemical vapor deposition, ultrasonication, laser ablation, mechanical exfoliation[14,41], while metals and alloys are generally prepared by reducing corresponding metal ions or metal oxides via chemical, electrochemical, or photochemical approaches[23,24,52]. The synthesis of organic frameworks is more complicated because the reaction condition must allow the formation of well-defined building blocks while avoiding the decomposition of organic linkers[59]. Besides room-temperature synthesis routes, the electric heating, microwave, mechanochemistry, electrochemistry, and ultrasonic techniques have also been exploited for preparing MOFs and COFs[59-61].

Distinctively, light absorbers in homogeneous photocatalytic systems represents the photosensitizer. Metal (such as ruthenium, iridium, platinum, and copper) complex

photosensitizers, which are prepared via a series of organic reactions, are the most widely used, owing to their various excited-state electronic configurations and long-lived triplet states[62-65]. In addition, organic photosensitizers (without any metals) have been developed and optimized via molecular engineering to attain the desirable solubility, stability and lifetime of excited states[64,66]. Furthermore, carbon nanodots, which possess tunable surface chemistry, low toxicity, and scalable synthetic routes, are an alternative to those molecularly defined complexes[67]. Carbon nanodots are synthesized via either top-down approaches with the breakdown of graphite, graphene or soot, or bottom-up approaches by thermally decomposing cheap organic molecular precursors or polymers[67,68].

[H3] Cocatalysts

Cocatalysts in heterogeneous photocatalytic CO_2 reduction processes may play crucial roles[5,69,70]. Firstly, they can improve the separation and migration of photo-generated electrons and holes, and thus enhance the activity. Secondly, they can help to lower the activation energy or overpotentials of CO_2 conversion process to improve the reaction kinetics and can direct the selectivity of CO_2 reduction toward a desired product. Furthermore, cocatalysts can suppress parasitic side reactions, such as H_2 evolution reaction, and enhance the robustness of the photocatalysts for long-term processes by efficiently consuming the photo-generated electrons (for CO_2 reduction) and holes (for the counter water/substrate oxidation).

The major cocatalysts applied for heterogeneous photocatalytic CO_2 reduction include metals[32,71-73] and alloys[74,75]; metal compounds[5] such as metal oxides[76,77], metal hydroxides[78], metal sulfides[79], metal carbides[80], and metal nitrides[81]; graphene-based materials[46,82]; enzymes[83-88]; bacteria[89-91]; and metal complexes[19,39,49,92,93]. In addition, surface defects can be created as pseudo co-catalysts which serve as catalytically active sites[35,38,53,94,95]. . Metal compound cocatalysts are synthesized via various approaches such as hydro/solvo-thermal reactions[76,79] and high-temperature gas-solid reactions[81]. Graphene-based cocatalysts are generally formed in-situ on light absorber via chemical vapor deposition or hydrothermal reaction, resulting in an ideal face-to-face interfacial connection[46,82]. Common enzymes applied for CO_2 reduction include CO dehydrogenase and formate dehydrogenase[83-85], whose preparations require laborious purification[98,99]. Elaborately designed enzymes can be fabricated through genetic engineering and overexpression[86,87]. To eliminate the extensive purification process of isolating enzymes, bacteria cocatalysts such as *Moorella thermoacetica*[91,100] and *Sporomusa ovata*[90] have been directly used. They are purchased and inoculated in a growth medium for a certain time prior to assembling with the light absorber. Metal complexes can be applied as the cocatalyst for a semiconducting light absorber in heterogenous photocatalytic CO_2 reduction[31,49-51] or an independent catalyst (namely, molecular catalyst) in homogeneous photocatalytic CO_2 reduction[31,50,101-103], whose synthesis

is based on serial organic reactions[63,64].

Assembling of light absorber and cocatalyst might be a separate step following their syntheses or a simultaneous process during the synthesis of either component. As a separate step after syntheses, the assembly is realized via wet mixing (stirring or grinding till dry)[76,79], chemical reaction[50,51,104], electrostatic coupling[93], bioprecipitation (for bacteria and enzymes)[88,89,91]. The simultaneous synthesis and assembly is beneficial for enhancing interfacial contact and thus allowing efficient charge transfer across the interface[5]. Metallic cocatalysts are typically simultaneously synthesized and assembled with the light absorber to ensure an intimate contact[5,96]. Namely, the metal ion precursor is reduced and loaded onto the light absorber using deposition techniques such as chemical deposition, photo-deposition and electro-deposition [5]. Alternatively, a three-step process of wet impregnation, calcination and reduction can be routinely employed[73,97]. For conventional homogenous photocatalytic systems, the light absorber (photosensitizer) and molecular catalyst (metal complexes) are independently dispersed in the solvent[63,64]. Alternatively, molecular photosensitizer can be covalently bonded to the catalyst complex as a multi-nuclear supramolecular photocatalyst with linkages such as -CH_2-CH_2-, -CH=CH-, -CH_2-O-CH_2-, and -CH_2-CH(OH)-CH_2-[30,105].

[H3] Catalyst stability/recyclability

An ideal catalyst for photocatalytic CO_2 reduction can maintain its excellent performance for a long time in terms of both activity and selectivity. On the one hand, it exhibits a high stability in a long-term run lasting tens to hundreds of hours. On the other hand, it shows a great recyclability that allows multiple runs especially for batch reactions. The duration and cycle index are typically within 20 h and 3 h, respectively, which are still below a rigorous stability test. Furthermore, characterizing the spent catalyst is essential to confirm the robustness of the catalyst, and to help to understand the reasons for catalyst deactivation (if any).

[H2] Catalyst characterization

As-synthesized catalysts are characterized to clarify their structures, chemical states, optical properties and energy band positions. Catalyst properties can differ under reaction conditions, so operando characterizations are highly desirable though not readily available at present.

[H3] Structure determination

X-ray diffraction (XRD) can determine the crystal structure of the catalyst and can suggest its crystallite size (up to 100 nm) according to the Scherrer equation [106]. Scanning electron microscopy (SEM) and transmission electron microscopy (TEM) can be used to assess the morphological structure of the catalyst. TEM uses higher acceleration voltages than those

of SEM, resulting in smaller de Broglie wavelengths of electrons and hence higher resolutions for lattice spacing identification[107]. Furthermore, the energy dispersive X-ray spectroscopy, electron energy loss spectroscopy, and high-angle annular dark-field imaging that are available on electron microscopes allow the spatially resolved elemental analysis[108]. In addition, scanning probe microscopies such as atomic force microscopy and scanning tunnelling microscopy (STM) are widely employed to reveal the thickness of 2D materials[109]. The surface area and pore volume of catalysts are measured via gas adsorption-desorption (primarily N_2) and calculated based on Brunauer-Emmett-Teller theory and Barrett-Joyner-Halenda model, respectively[110]. Moreover, the adsorption-desorption of CO_2 and its temperature dependency explored via temperature-programmed desorption indicate the quantity and strength of active sites[111]. The defects/vacancies in inorganic-semiconductor-based catalysts are characterized via electron paramagnetic resonance (EPR) spectroscopy based on unpaired electrons[112].

[H3] Chemical states

The chemical states of catalysts are mainly explored via spectroscopy The chemical environment of elements is assessed by X-ray photoelectron spectroscopy (XPS) and X-ray absorption spectroscopy (XAS). The detection depth of XPS is below 10 nm as photoelectrons generated in the bulk catalyst are highly likely to be recaptured when traveling through the sample into the vacuum[113]. In contrast, XAS offers information for both the bulk and surface. In XAS, X-ray absorption near edge structure spectroscopy is generally used to determine oxidation states and extended X-ray absorption fine structure spectroscopy can be used to investigate coordination and bonding properties[114]. The chemical structure of metal complex catalysts is characterized via nuclear magnetic resonance (NMR) spectroscopy and mass spectrometry (MS)[115].The chemical structures of intermediate species formed during the synthesis of catalysts should also be confirmed. The asymmetric vibrations of polar groups and the symmetric vibrations of nonpolar groups are detected via Fourier transform infrared (FT-IR) spectroscopy and Raman spectroscopy, respectively, which are powerful tools to elucidate the functional groups and chemical structures of catalysts[116].

[H3] Optical properties

The characterization of optical properties is essential for photocatalysts. The wavelength-dependent light absorption ability of catalysts is measured via ultraviolet-visible (UV-vis) spectroscopy and the band gap can be derived from the resulting Tauc plot[117]. The behaviours of photo-generated charge carriers are studied by transient absorption spectroscopy (TAS), surface photovoltage spectroscopy (SPS), photoluminescence spectroscopy (PLS) and photoelectrochemical tests of photocurrent and electrochemical impedance spectroscopy (EIS). TAS measurements from picosecond to second time scales imply the dynamics of charge generation, recombination, and interfacial charge transfer[118]. In contrast, SPS and PLS are used

to solely investigate charge redistribution and charge recombination, respectively[110]. Both SPS and PLS have the steady-state and transient forms, suggesting the event count and kinetics, respectively. In addition, photocurrent and EIS measured by irradiating the working electrode (coated with catalyst) can reveal the population of active charge carriers and the resistance of charge transfer in electrode and across electrode-electrolyte interface, respectively[28,119]. Moreover, the excited-state redox potential of photosensitizers applied in homogenous catalytic processes can be determined by phase-modulated voltammetry[120] or using the Rehm-Weller formalism based on the electron emission spectrum and ground-state electrochemical properties acquired via cyclic voltammetry[121].

[H3] Energy band positions

The energy band positions of catalysts are identified to check if the thermodynamic requirements of photocatalytic CO_2 reduction are satisfied. The first step is to locate the Fermi level, which is generally measured as the flat-band potential versus a reference electrode by constructing Mott-Schottky plots via electrochemical tests. Generally, the Fermi level is close to CBM for n-type semiconductors and VBM for p-type semiconductors, but this is not quantitative [122]. Instead, the position of VBM is determined by valence-band XPS, which is referenced to the Fermi level (zero point of binding energy). Afterward, the position of CBM is obtained based on the position of VBM and the band gap derived from UV-vis spectroscopy.

[H2] Experimental setup

The reactors for photocatalytic CO_2 reduction are categorized into batch reactors and flow reactors (**Fig. 3)**. All reactors require an optical window that allows light irradiation on catalysts from a light source. The light sources most employed in laboratories are the xenon arc lamp, mercury vapor lamp, and light-emitting diode (LED) lamp. Xenon lamps offer smooth sun-like emissions from UV to visible spectrums with characteristic wavelengths emitted in 750-1000 nm. Equipping a Xenon lamp with an AM1.5G optical filter makes a viable solar simulator and the standard light source of photocatalytic processes at a controlled light intensity of 100 mW cm^{-2}. In contrast, mercury lamps demonstrate high-intensity spectral lines emitted in deep UV to visible light regions, while LED lamps emit light in a very narrow band of wavelengths that is dependent on the energy band gap of the semiconductor applied to make the LED. Moreover, multiple optical filters besides AM1.5G filter are commercially available, such as bandpass filters, longpass filters and shortpass filters. These filters provide various lights for investigating the contributions of lights with different wavelength distributions. Furthermore, it is a good choice and goal to perform field tests with utilizing natural sunlight as the light source.

Batch reactors are applicable for both heterogenous and homogenous reactions and are generally operated in the solid-gas mode (**Fig. 3a**), solid-vapor mode (**Fig. 3b**), solid-liquid-gas mode (**Fig. 3c**), or liquid-gas mode (**Fig. 3d**). In the solid-gas mode, the reductant is in a gaseous

phase (such as H_2 and CH_4), while in solid-vapor mode, the reductant is in vapor phase (such as H_2O vapor). In each mode the solid catalyst is coated on a support such as glass slide/dish[32,38,71,123], Teflon holder[77], SiO_2 disk[73,97], Nickel foam[124] or Aluminium plate[123]. Some supports, such as SiO_2 disk[73,97], have unique microstructures that provide a light-diffuse-reflection surface to enhance the redirection and utilization of incident light[125]. In solid-liquid-gas mode, the reductant is in liquid phase or a solvent is present (**Fig. 3c**) and the catalyst powderis dispersed in liquid under continuous stirring. However, this mode suffers from limited exposure of catalysts to CO_2 because of the low solubility of CO_2 in most liquids (representatively, H_2O)[77,126] and low light utilization efficiency, owing to the absorption and scattering by liquid[127]. Furthermore, homogenous photocatalytic CO_2 reduction is performed in liquid-gas mode, where the solution contains molecular catalyst, photosensitizer, reductant and dissolved CO_2 (**Fig. 3d**).

Unfortunately, Re-adsorption and back or side reactions are highly likely to occur in batch reactors, owing to the continuous accumulation of products , resulting in reduced yields[128]. In contrast, flow reactors ensure the movement of reactants and products at a constant flow rate but suffer from short residence time. Flow reactors are used for heterogenous photocatalytic CO_2 reduction, and the inlet gas is a mixture of CO_2 and reducing gas or bubbled CO_2 through a reducing liquid such as H_2O. The catalyst powders are coated on a support, which, from the macroscopic perspective, can be defined as a planar support (**Fig. 3e**), monolith support (**Fig. 3f**), or optical fibers (**Fig. 3g**). Monolith supports generally have a honeycomb structure and a high surface-area-to-volume ratio with many internal channels (**Fig. 3f**), enabling sufficient contact between reactants and catalyst and low pressure drop with high flow rate[129]. However, owing to the opacity of monolith, light cannot efficiently penetrate through the long channels[127]. In addition, optical fiber can be used as a medium to uniformly and efficiently deliver light to the catalyst coated on its surface (**Fig. 3g**), whereas the adhesion strength of catalyst is low and the effective surface area is small[130,131]. Inserting optical fibers into the honeycomb structure of a monolith support can address the above issues, thus being a promising architecture with hybrid supports[132,133].

[H2] Operation conditions

The operation conditions can be adjusted to optimise the photocatalytic performance. Essential operational variables include light source, temperature, reductant, feed ratio and flow rate (for flow reactors), pressure, catalyst dosage, reaction time, solvent (if any) and its pH. Firstly, the light source represents wavelength distribution and light intensity. Wavelength distribution is tuned by using various lamps or applying various optical filters on one lamp, while light intensity is controlled by the output power and distance between the lamp and catalyst. Light irradiation causes a temperature rise. Synergetic thermo-photo catalysis with external temperature control allows operations in a wide temperature range, presenting a new

way to optimizing catalytic performance[73,97]. Alternatively, for fundamental studies, the temperature rise may be suppressed by equipping IR optical filters with a water cuvette.

The reducing capability and affinity to catalysts varies amongst reductants Furthermore, the reductant-to-CO_2 feed ratio can impact photocatalytic performance, especially selectivity. The pressures of CO_2 and reducing gas should also be considered. Although a higher pressure contributes to molecular adsorption and favours a reaction with less produced moles than converted moles, it may cause less efficient use of feedstock and some safety issues. Catalyst dosage can be adjusted to maintain a desirable catalytic efficiency. Another operation condition to consider is reaction time, which represents reaction duration for batch reactors and residence time for flow reactors. Reaction time can beoptimized for an efficient forward reaction of CO_2 reduction, while supressing backward and side reactions. Solvent should be carefully chosen based on its dissolving capacities for CO_2, reducing agent, catalyst, photosensitizer and products. The pH of the solvent, which directly relates to the concentration of protons, is also an important operational variable.

Furthermore, it is necessary to perform negative control experiments, namely, tests in the absence of light irradiation (at the same temperature), CO_2 (using argon instead), reductant, catalyst (leaving the blank support if used), photosensitizer, or solvent. The negative control experiments should result in negligible yields. Nevertheless, to obtain solid evidence that the results are not artefacts especially when the amount of products is small, a complete and reproducible $^{13}CO_2$ labelling experiment is required.

[H2] Measurements

The assessment of photocatalytic CO_2 reduction performance requires product analysis, quantum/energy efficiency measurement, catalyst stability/recyclability evaluation, and confirmation by isotopic labelling experiment. Multiple products might be generated, and their quantifications involve several techniques. Gas chromatography (GC) with a thermal conductivity detector is used to detect the unreacted CO_2, produced CO and CH_4, and by-products such as H_2 and O_2. Moreover, the flame ionization detector (FID) equipped on a GC shows a high sensitivity to hydrocarbons such as CH_4, C_2H_6 and C_2H_4 and alcohols such as CH_3OH and CH_3CH_2OH. In addition, GC-FID can quantify low-level CO and CO_2 if a Ni-catalyst-packed methanizer is installed. NMR spectroscopy with solvent suppression[53] is a powerful tool to measure liquid oxygenate products, including alcohols , aldehydes, and acids[134]. The difficulty of analysing HCHO can be overcome by using a trapping agent ($NaHSO_3$)[134]. Other than NMR, liquid chromatography and ion chromatography can detect acid products such as HCOOH, CH_3COOH and $H_2C_2O_4$. Furthermore, the coupling of GC and provides a high accuracy for measuring almost all common products and unreacted CO_2, though the use of multiple chromatographic columns might be required[72]. In GC-MS, all substances should be properly separated, otherwise the fragmentation patterns cannot be properly interpreted and labelling

studies may lead to wrong conclusions.

Some specific measurements are needed to obtain the essential metrics for evaluating a photocatalytic CO_2 reduction process. To obtain apparent quantum efficiencies, a series of monochromatic lights with definite wavelengths are employed as the light source by equipping bandpass filters on the lamp or directly using LED lamps. The solar-to-chemical efficiency is acquired using AM1.5G simulated sunlight. In both cases, light intensity, irradiation area, and product yields should be measured. In addition, for heterogenous photocatalysis, catalyst stability in a flow reactor can be evaluated with a long-term photocatalytic test by continuously monitoring product yields, and catalyst recyclability in a batch reactor is assessed by reusing the catalyst for multiple runs and measuring product yields for each run. The catalyst might be regenerated via washing with deionized water or heat treatment. For homogenous photocatalysis, catalyst stability is investigated by performing tests for a long duration with product quantification at a certain time interval[63]. It is highly recommended to perform $^{13}CO_2$ labelling experiment and analyse the products by a suitable method such as GC-MS, NMR spectroscopy, or FT-IR spectroscopy to confirm incorporation of ^{13}C into the product. Nevertheless, there are exemptions given a large amount of carbon-containing substances are continuously produced in a long duration in flow reactors.

[H2] Mechanism exploration

[H3] Experimental techniques

The exploration of photocatalytic CO_2 reduction mechanisms mainly covers two aspects, namely, charge behaviours (charge generation, separation, and migration) and chemical reaction pathway..

XPS and XAS can detect the change in the chemical environment of catalyst elements induced by illumination or reactants, which suggests the change in electron density and corresponding charge behaviours[23,57,135,136]. For catalysts with intrinsic or photo-induced paramagnetic responses, EPR measurements can be performed alongside XPS and XAS by comparing the signal intensities obtained with and without illumination or reactants[55,137,138]. Furthermore, the coupling of operando scanning fluorescence X-ray microscopy and environmental TEM enables the investigation of electronic structure change at single-particle level[137]. In addition, Kevin probe and Mott-Schottky measurements reveal Fermi level and hence the interfacial band bending upon contact[135]. For homogenous photocatalytic CO_2 reduction, UV-vis, XAS, TAS, IR, and Raman spectroscopies help to reveal the charge transfer and electron donation/reception of the photosensitizer and molecular catalyst[63,139-141]. Time-resolved spectroscopies are complementary to these techniques, particularly for photophysical steps and charge transfer steps.

Identifying reaction intermediates is an effective approach for depicting the chemical reaction pathway. In-situ irradiated diffuse reflectance infrared Fourier transform

spectroscopy is a powerful technique to detect adsorption-state intermediates and products such as monodentate carbonate (m-CO_3^{2-}), bidentate carbonate (b-CO_3^{2-}), *HCO_3, *COO, *COOH, *CHO, *CO, and *OCH_3[38,46,94,142], while EPR spectroscopy allows the identification of radical intermediates which are typically unstable and have an unpaired electron, such as •CO_2^-, •COOH, •CHO, •O_2^-, and •OH[135,143]. Steady-state isotopic kinetic analysis can be coupled with in-situ techniques to give more accurate and detailed results[142]. Moreover, advanced STM enables mechanism investigation at single-molecule level[144]. Namely, the CO_2 dissociation process is visualized after injecting electron(s) from STM tip to adsorbed CO_2, and the threshold energy for electron-induced CO_2 dissociation is acquired by analysing bias-dependent dissociation yields. Furthermore, the thermodynamic parameter, reaction order, influence of diffusional step on kinetics, and role of proton donor are also important for understanding reaction pathway.

For plasmonic catalysis, there is one more essential task, namely, identifying the thermal and hot-carrier contributions in the catalytic process. This can be achieved by exploring the dependences of reaction rate and quantum efficiency on light intensity, comparing the kinetic isotope effects under illumination and in dark, and electron quenching, in combination with some advanced in-situ characterization techniques[145,146].

[H3] Theoretical calculations

First-principles computational chemistry, especially density functional theory (DFT), is most widely used to explore the photocatalytic CO_2 reduction mechanism. DFT calculations are usually performed on pristine catalysts to identify band structure and electronic excitation. Furthermore, DFT can predict catalyst interactions with CO_2, intermediates and products to determine parameters such as the adsorption geometry and energy, change in Gibbs free energy, transition state, reaction barrier, and rate-determining step[72,147-149]. Van der Waals correction and spin polarization are employed, and the solvation model is needed if solvent is involved[40]. Besides, light irradiation effect is modelled via time-dependent DFT method or kinetic Monte Carlo simulation[150,151]. All possible paths should be considered, calculated, and compared based on both thermodynamics (Gibbs free energy) and kinetics (energy barrier of transition state)[35,149].

Machine learning, as an emerging data-driven computational method for modelling and interpreting complicated multi-dimensional relations, has been adopted as a complement of the time- and resource-intensive first-principles calculations[152]. Machine learning is used to screen elementary steps and preclude the pathways involving steps predicted to have extremely high barriers[153,154]. However, current application of machine learning techniques is still limited, owing to the lack of sufficient data[152].

[H1] Results

There are six important numeric metrics in photocatalytic CO_2 reduction processes that should be obtained and reported, including the production rate, selectivity, CO_2 conversion rate, turnover number/frequency, (apparent) quantum efficiency, and solar-to-chemical efficiency. **Fig. 4** summarizes these numeric metrics of forty photocatalysts from seven groups to illustrate the general results of interest and the best practice (among these studies). Each metric will be discussed in detail in the corresponding subsection regarding its calculation, analysis, and optimization. When optimizing the operation condition, one should have an overall view of all facets of the performance by considering a matrix of metrics. For example, applying a large light intensity might enhance the production rate, CO_2 conversion rate and turnover number/frequency but reduces quantum efficiency and solar-to-chemical efficiency. In addition, catalyst stability in a long-term run and catalyst recyclability that allows multiple runs are also essential metrics. Furthermore, the most common mechanisms of photocatalytic CO_2 reduction will be elucidated at the end of this section.

[H2] Production rate

Production rate describes catalytic activity. Taking the effectiveness of time and material into account, production rate is calculated via **Eqn. 1** with a recommended unit of μmol h^{-1} g_{cat}^{-1}.

$$Production\ rate\ (\mu\text{mol}\ \text{h}^{-1}\ \text{g}_{cat}^{-1}) = \frac{Yield\ over\ a\ period\ of\ time\ (\mu\text{mol})}{Time\ (h) \times Mass\ of\ catalyst\ (g)} \quad (1)$$

This metric is best suited for heterogeneous systems but can be applied to all photocatalytic CO_2 reduction processes. Turnover number and turnover frequency are preferred for homogeneous systems since the exact number of active sites is known. Comparison between homogeneous and heterogeneous systems remains challenging. As shown in **Fig. 4a**, CO is the most common product of CO_2 reduction, with a wide range of production rates from 1 to ~10^6 μmol h^{-1} g_{cat}^{-1}. Moreover, some photocatalysts contribute to the production of HCOOH and CH_4 while the production rates are generally below ~10^4 μmol h^{-1} g_{cat}^{-1}. In addition, CH_3OH and multi-carbon substances (such as C_2H_4[155], CH_3CHO[37], and CH_3COOH[90]) are formed over some inorganic-semiconductor-based photocatalysts, most of which are at the rate of 10~10^4 μmol h^{-1} g_{cat}^{-1} except CH_3OH production over Cu_2O catalyst[137]. Furthermore, this plot suggests the higher activity of molecular catalysts and enzymes than others toward the generation of carbon-containing substances. The plasmonic catalysts also demonstrate impressive production rates while large light intensities are commonly used.

Production rate can also be expressed as the areal activity to illustrate the effectiveness of irradiation area and can be calculated via **Eqn. 2**.

$$Production\ rate\ (\mu mol\ h^{-1}\ cm_{cat}^{-2}) = \frac{Yield\ over\ a\ period\ of\ time\ (\mu mol)}{Time\ (h) \times Irradiation\ area\ on\ catalyst\ (cm^2)} \quad (2)$$

This metric is very meaningful when the catalyst itself exhibits as a film or powdered catalyst is coated on a substrate toward promising solar panel technologies for solar-to-chemical conversion[156]. To improve the production rate, the number of active sites and activity of each active site should be enhanced, which require an elaborate design of catalysts.

[H2] Selectivity

Selectivity towards high-value products is desired in terms of economic and environmental benefits. A high selectivity (preferentially 100%) also eliminates or reduces the energy consumption and cost for separating and purifying products. Selectivity is defined as the ratio of the yield of a target product to the sum of the yields of all products (**Eqn. 3**).

$$Selectivity = \frac{Yield\ of\ target\ product\ (\mu mol)}{Yields\ of\ all\ products\ (\mu mol)} \quad (3)$$

The products typically represent the carbon-containing substances resulting from CO_2 reduction.H_2 should also be accounted for if water or other proton source is used as the reductant or reaction medium. **Fig. 4b** summarizes the selectivity among carbon-containing substances, suggesting the realization of inspiring selectivity of 100% for various products[21,23,38,54,57,157]. Nevertheless, simultaneous generation of multiple products with limited selectivities is still a common phenomenon (particularly, CO and CH_4)[55,69,158]. Besides, selective production of multi-carbon species remains a huge challenge over the currently dominant C1 chemicals. Moreover, the competitive H_2 evolution reaction further limits the selectivity in numerous studies[62,64,72,159].

Catalytic selectivity highly depends on the interactions between the molecule and catalytically active site[15,63]. It is hard to clarify which group of catalysts shows higher selectivities. While, organic-related catalysts (MOFs/COFs, molecular catalysts, bacteria, and enzymes) and low-dimensional inorganic catalysts have more defined and modulable molecular structures that allow the precise control of active sites, thus more likely to realize high selectivities. However, it remains a challenge to achieve the reduction of CO_2 beyond two electrons.

[H2] CO_2 conversion rate

The CO_2 conversion rate is a critical metric that has not received much attention, but should be included as an essential metric in the assessment of photocatalytic CO_2 reduction systems. It reflects the effectiveness of CO_2 feedstock utilization, which is calculated via **Eqn. 4**.

$$CO_2\ conversion\ rate = \frac{Amount\ of\ reacted\ CO_2\ (\mu mol)}{Amount\ of\ fed\ CO_2\ (\mu mol)} \quad (4)$$

Besides the nature of the catalyst, the CO_2 conversion rate is also affected by the total amount

of available CO_2, reaction time for batch reactors and CO_2 flow rate for flow reactors. CO_2 conversion rate should be calculated when chemical equilibrium is reached. Currently, most processes demonstrate tiny CO_2 conversion rates below 1% as a large substrate access is provided to the systems. CO_2 conversion rates higher than 10% have been attained using low-concentration CO_2 feedstock at 300~1000 ppm over inorganic-semiconductor-based photocatalysts as important practices toward CO_2 conversion in air (**Fig. 4c**)[69,71]. Ultimately, close-to-unity conversion rates are desirable to avoid energy penalties and CO_2 release into the atmosphere.

[H2] Turnover number/frequency

Turnover number (TON) (**Eqn. 5**) and turnover frequency (TOF) (**Eqn. 6**) are two important metrics to quantify the catalytic activity of each active site. To reflect the real rate of catalytic systems, TOF may be derived from the slope of the TON-time curve instead of the mean value over the whole duration.

$$Turnover\ number = \frac{Number\ of\ reacted\ CO_2}{Number\ of\ active\ sites} \quad (5)$$

$$Turnover\ frequency\ (h^{-1}) = \frac{Number\ of\ reacted\ CO_2}{Number\ of\ active\ sites \times Time\ (h)} \quad (6)$$

For homogeneous catalytic systems with molecular catalysts, the number of active sites is well defined. However, for heterogenous catalytic systems, the identification and quantification of active sites are challenging. As an approximation, cocatalyst such as metal nanoparticle is generally regarded as active site. As summarized in **Fig. 4d**, most TONs were measured in a short period of time (< 15 h) with a wide distribution from 10^{-5} to 10^{3}. Long-term measurements up to 120 h were performed for some catalysts, demonstrating larger TONs from ~1 to 10^{4}. Moreover, molecular catalysts seem to be more active with larger TONs and TOFs than other catalysts, owing to their effective utilization. For example, the Cu-PP/Fe-TDHPP catalyst realized impressive TON of 16,109 and TOF of 700 h^{-1}[62].

[H2] Quantum efficiency

Quantum efficiency (or quantum yield) is an essential numeric metric to describe the effectiveness of converting photons to active electrons that participate in reactions. There are two quantum efficiencies, namely, internal quantum efficiency (IQE) based on absorbed photons by catalyst and external/apparent quantum efficiency (EQE/AQE) based on incident photons. Although IQE better illustrates the intrinsic properties of catalysts, EQE/AQE is of greater practical significance and easier to measure, thus having been widely employed to evaluate photocatalytic processes. **Eqn. 7** illustrates the classic formula and convenient formula for EQE/AQE calculation, where the number of electrons required to reduce CO_2 is 2 for CO, HCOOH and $H_2C_2O_4$, 4 for HCHO, 6 for CH_3OH, 8 for CH_4 and CH_3COOH, 10 for CH_3CHO, 12 for C_2H_5OH and C_2H_4, and 14 for C_2H_6.

$$Apparent\ quantum\ efficiency = \frac{Number\ of\ electrons\ for\ CO_2\ reduction}{Number\ of\ incident\ photons} =$$

$$\frac{\sum(Number\ of\ produced\ x\ molecule \times Number\ of\ electrons\ required\ to\ reduce\ CO_2\ to\ x)}{Light\ intensity\ (W\ m^{-2}) \times Irradiation\ area\ (m^2) \times Time\ (s) \div \frac{Planck\ constant\ (J{\cdot}s) \times Light\ speed\ (m\ s^{-1})}{Wavelength\ (m)}} =$$

$$\frac{33.2296 \times \sum[Yield\ of\ x\ (\mu mol) \times Number\ of\ electrons\ required\ to\ reduce\ CO_2\ to\ x]}{Light\ intensity\ (mW\ cm^{-2}) \times Irradiation\ area\ (cm^2) \times Time\ (h) \times Wavelength\ (nm)} \quad (7)$$

Fig. 4e illustrates the wavelength-dependent AQEs for various catalysts. While most AQEs remain below 10%, significant AQEs up to ~28% in the visible-light range have been reported over Cu_2O[137] and Ir-QPY/Co-Pc[159] catalysts. To improve AQE, the catalyst should demonstrate broad and intense light absorption, and photo-generated charge carriers can be efficiently separated and migrated to induce surface reactions.

[H2] Solar-to-chemical efficiency

Solar-to-chemical (STC) efficiency is utilized to quantify the efficiency of energy conversion from solar energy to stored chemical energy (**Eqn. 8**).

$$\text{Solar to chemical efficiency} =$$

$$\frac{\sum[Yield\ of\ x\ (\mu mol) \times Gibbs\ free\ energy\ change\ of\ reducing\ CO_2\ to\ x\ (kJ\ mol^{-1})]}{Light\ intensity\ (mW\ cm^{-2}) \times Irradiation\ area\ (cm^2) \times Time\ (s)} \quad (8)$$

When the Gibbs free energy change of a reaction is positive, the STC efficiency provide a positive value. When the Gibbs free energy change is negative, the STC efficiency will have a negative value and not reflect the economic value of a solar chemical process. For example, Photocatalytic CO_2 reduction processes with sacrificial reagents (strong reductants) do not have valid STC efficiencies as the chemical energy is released but not stored under illumination. Unfortunately, only a small number of papers have reported the STC efficiencies, which are below 1% (**Fig. 4f**), far from the industrial requirement. The same strategies to improve AQE can be employed to enhance STC efficiency.

An alternative value-oriented metric of solar-to-value (STV) rate can be reported by subtracting the total cost of reactants from the total value of products per unit time per unit irradiation area (considering practical solar utilization) (**Eqn. 9**)[156].

$$\text{Solar to value rate} =$$

$$\frac{\sum[Value\ of\ x\ (\$\ \mu mol^{-1}) \times Yield\ of\ x\ (\mu mol)] - \sum[Cost\ of\ y\ (\$\ \mu mol^{-1}) \times Consumption\ of\ y\ (\mu mol)]}{Time\ (h) \times Irradiation\ area\ (cm^2)} \quad (9)$$

The cost of CO_2 is negative due to carbon taxes, whereas the costs of most sacrificial reagents are much higher than the values of CO_2 reduction products and the oxidation product of the sacrificial reagent. The STV metric may be expanded with including the costs of feedstock pretreatment, product collection and separation, catalyst preparation, and scaling factors. This requires a comprehensive techno-economic analysis.

[H2] Photocatalytic mechanism

Photon absorption and subsequent charge transfer can promote the photocatalyst and other components in the system to the excited state., The molecules reconfigure to accommodate the excited-state potential energy surfaces, driving the chemical transformation with lower activation barriers[17]. The excited state cannot simply be described using the ground-state theory and characterizations, so a thorough understanding of the excited-state dynamics is the key to exploring the photocatalytic mechanism.

The mechanism of photocatalytic CO_2 reduction is typically expressed in terms of charge behaviour and reaction pathway. The charge transfer directions of the light absorber, cocatalyst, and reactant are highly dependent on energy band position, photon energy, molecular adsorption, and redox potential. After identifying charge transfer directions, heterostructure catalysts can be identified as p-n junction or Z-scheme, both of which allow more efficient charge separation than their single components[5]. The most common reaction routes of heterogenous photocatalytic CO_2 reduction to C1 products are summarized in **Fig. 5**, including the oxygen-atom-connecting monodentate or bidentate intermediate route with the direct protonation of CO_2 by H^+ from solution or CO_2 insertion into X-H bond (**Fig. 5a**)[1]; the surface-bound bicarbonate intermediate route via the reaction between CO_2 and surface -OH group (**Fig. 5b**)[160]; the $\bullet CO_2^-$ radical intermediate route with the following formaldehyde pathway or carbene pathway (**Fig. 5c**)[161]; and the glyoxal intermediate route in which the dimerization of *CHO into glyoxal is followed by sequential reactions to form *CH(OH)(CHO), CH_2(OH)(CHO), *CH_2(CHO), CH_3CHO, *CO(CH_3), CO + *CH_3, and CH_4 (**Fig. 5d**)[1]. For the formation of multi-carbon products, C-C coupling is the key step. For example, pathways toward C_2H_4 and C_2H_6 go through coupling of *CH_2 and *CH_3 intermediates (carbene pathway), while the coupling of *CHO intermediates (glyoxal pathway) can produce a variety of C1 and C2 oxygenates[162]. The mechanisms of homogenous photocatalytic CO_2 reduction are quite different, and η^1-CO_2 adduct and hydride complex are believed the most common intermediates[29].

It should be noted that theoretical calculations cannot really predict or demonstrate the photocatalytic mechanism. Firstly, the complex photocatalytic CO_2 reduction system cannot be rigorously modeled, especially for light irradiation, catalyst structure and solvation effect. Secondly, current calculation methods are not yet able to accurately model the energy surfaces to find the free energy reaction pathways in excited states. Therefore, the calculation results should only serve as an auxiliary reference of experimental results.

[H1] Applications

Currently, photocatalytic CO_2 reduction is mainly pursued in academic laboratories, but it may be ultimately applied to valorize atmospheric CO_2, emission streams from thermal power stations and iron factories, and exhaust gases of vehicles[163]. In this section, the considerations

for practical application of photocatalytic CO_2 reduction will be discussed together with a few examples of application.

[H2] Considerations for practical application

There are seven major considerations for the practical application of photocatalytic CO_2 reduction processes. The first consideration is the CO_2 source, which is normally atmosphere and emission streams[163,164]. Different CO_2 sources have different CO_2 concentrations down to ppm level and different interfering species (such as O_2, N_2, SO_2, and H_2O) that might compete with CO_2 for molecular adsorption and chemical reactions[40,69,71]. Therefore, additional processes of CO_2 capture and purification prior to photocatalytic reactions might be needed.

The second consideration is the availability of solar energy because only in sunny daytime can solar energy be utilized to drive reactions[17]. In addition, sunlight intensity varies with location and weather, so solar concentrators might be installed[123]. This limited solar ebergy only allows for intermittent operations[72] unless solar energy is stored as electric energy in the daytime, which then provides illumination via lamp at night[17,165]. A persistent photocatalytic system was recently proposed to store charges in a capacitor or battery-like material that interfaces with a photocatalyst during illumination and discharge after illumination to continue driving a catalytic reaction[166].

The third consideration is the scale-up of the photocatalytic reactor. Since mass and photon transfers are highly dependent on scale, the optimal reactor geometry, window material and thickness and catalyst architecture in bench-scale tests might not be applicable for a large scale[8,167]. Accurately modelling mass, photon and heat transfers for optimizing large-scale reactors is a promising approach to address this issue[8,168].

The fourth consideration is the separation and collection of products. There is often a mixture of products and reactants (CO_2 and reductant) are not fully consumed, requiring the separation for downstream utilization. The installation and operation of separation systems such as membrane system and extraction system would lead to additional cost and energy consumption. In addition, developing a tandem reaction system to utilize products on site is another solution[169,170].

The fifth consideration is cost effectiveness, which is evaluated through techno-economic assessment based on modelling of detailed processes with rational boundary conditions[8,164,171]. Non-technical factors that determine economic viability such as up-to-date political framework, supply chain partnership, consumer behaviour and labour force optimization, should be considered as well[172]. The result should be compared with those of other CO_2 capture and utilization technologies.

The sixth consideration is environmental impacts, which are quantified via life cycle assessment following ISO Standard 14040/14044 series[173]. Life cycle assessment covers fossil fuel depletion, global warming potential, ozone depletion, smog formation, acidification,

eutrophication, ecotoxicity andhuman health[173,174].

The last consideration for the scale up of photocatalytic CO_2 reduction processes is the system life span, which directly influences the economic and environmental benefits. The cost, labour, and environmental impacts associated with system maintenance and upgrading should be accounted as well.

[H2] Application examples

Photocatalytic CO_2 reduction has been appliedto several chemical processes, though they remain at the laboratory stage. The sunlight-driven reduction of CO_2 by H_2O is the most attractive application for realizing scalable energy storage and carbon-neutral production of high-energy-density fuels with O_2 as the only byproduct[175,176]. Moreover, photocatalytic CO_2 reforming of CH_4 is an essential application that allows the simultaneous treatment of two primary greenhouse gases with producing syngas as a versatile chemical feedstock[97,172,177,178]. Even ambient light irradiation can lower the reaction temperature by ~200 °C while maintaining similar efficiency relative to the thermal catalytic process[97]. Furthermore, photocatalytic CO_2 hydrogenation shows a great promise as the green alternative to conventional thermal catalytic reverse water-gas shift reaction, Sabatier reaction, as well as Fischer-Tropsch processes[6,35,179].

Current attempts toward the practical application of photocatalytic CO_2 reduction are mainly focused on the direct utilization of air as CO_2 feedstock[69,180,181] or natural sunlight as light source[72] whereas the reactors are still in bench scale. Inspiringly, a modular 5 kW pilot-scale solar-thermal catalytic system has been developed, which directly captured CO_2 and H_2O from ambient air and converted them to syngas first and further to drop-in fuels such as CH_3OH and kerosene under field conditions[182]. This setup is a valuable reference for practical photocatalytic CO_2 conversion although it ran via thermal catalysis so far. To apply for photocatalysis, slight modifications on the paraboloidal concentrator and replacement of catalyst are desired.

[H1] Reproducibility and data deposition

Data reporting and deposition are not standardized and reproduction of results across the field of photocatalytic CO_2 reduction remains a challenge. This section will discuss the factors affecting reproducibility and summarize the data reporting requirements and standard operation condition for comparing catalytic performances.

[H2] Factors affecting reproducibility

Firstly, the reproducibility is highly dependent on the structure and properties of catalysts. In heterogenous photocatalytic CO_2 reduction processes, the crystal phase, particle size, morphology, exposed facets and defects of catalysts directly influence CO_2 adsorption, light

absorption, charge separation and reaction pathway, hence photocatalytic efficiency[32,38,94,137,183]. Among these, defects are the most underrated yet the most important as they might cause up to 10-fold reduction in activity and quite different selectivities[35,38,53,94,95]. In homogenous processes, the exact structure and high purity of the molecular catalyst and photosensitizer must be ensured.

Secondly, carbon-based catalysts themselves or carbonaceous residues on the catalyst surface (resulting from catalyst preparation or adsorption of atmospheric volatiles) would impact the yield of carbon-containing substances[18,184]. For example, these carbon-based catalysts or carbonaceous residues might serve as the carbon feedstock for generating carbon-containing substances, rather than CO_2. Furthermore, carbonaceous residues can cover the active sites on the catalyst surface, thus inhibiting the adsorption and subsequent photocatalytic reduction of CO_2.

The shape, size and material of photocatalytic reactors directly affect mass, heat and photon transfers[8,167], leading to different results. Though some photocatalytic reactors have been commercialized, many researchers use home-made reactors. However, most reports simply present a scheme or photo of the reactor without detailed description of its dimensions and materials for walls and optical window, making it hard to reproduce the results.

The photocatalytic efficiency is strongly correlated to the light source. Different light sources have different spectra and intensities, providing photons with different energies in different quantities. The absorbed photons further determine the number of excited charge carriers for driving photocatalytic reactions[17]. Even for the same lamp, the spectrum and intensity will change with time.

[H2] Reporting requirements

Comprehensiveness and transparency are crucial for data reporting and deposition. The necessary data associated with photocatalytic CO_2 reduction and their definitions, reporting requirements, and reporting format regarding experimentation, catalyst characterization, photocatalytic performance, reaction mechanism, and carbon origin confirmation, are elaborated in **Table 2**. First, a comprehensive and detailed description of experimental procedures and setups is of vital importance to ensure the reproducibility. Particularly, a scheme or photo of the reactor should be provided with annotations on its dimensions and materials; and the model, spectrum and intensity of the light source should be reported. In addition, the reaction temperature should be *in-situ* probed via thermocouple or IR thermal imager. Moreover, the reporting of photocatalytic performance is based on seven metrics including production rates and selectivities of all products, CO_2 conversion rate, turnover frequency, apparent quantum efficiencies at various wavelengths, solar-to-chemical efficiency, and catalyst stability or recyclability. All metrics should be reported as the mean value with standard deviation derived from at least 3 parallel tests. Also, it is necessary to elucidate the

origin of the carbon in products by isotopic labelling experiment with $^{13}CO_2$, negative control tests and carbon balance calculation. Finally, schematic illustrations of the charge behaviours, energy band positions of catalyst, redox potentials, and chemical reaction pathway should be supplied based on experimental evidence. In addition, it is highly desired that the contributions of hot charge carriers and thermal energy in plasmonic catalytic processes can be distinguished.

[H2] Recommended catalytic performance evaluation standard

Although the optimization of operation conditions is encouraged, the results obtained under the standard operation condition should also be provided to compare data from different laboratories. The standard operation condition is proposed as follows. 100 mW cm^{-2} AM1.5G simulated sunlight applied as the light source, with the temperature monitored and reported (but not controlled) to simulate practical conditions. In terms of catalyst loading, 10 mg catalyst in 30 mL solvent (if required) is suggested. For batch reactors, 1 atm CO_2 is suggested, while for flow reactors a flow rate of 10 mL min^{-1} CO_2 should be used. The reductants have diverse chemical natures and phases, with a recommended dosage of 1 atm or 10 mL min^{-1} for gas reductants (such as H_2 and CH_4); 30 mL for liquid reductants (such as H_2O); or 20% volume fraction for solvate reductants (such as triethylamine). The reaction time is 2 h for batch reactors is 2h, while flow reactors should operate until stable activity is attained.

[H1] Limitations and optimizations

At present, photocatalytic CO_2 reduction suffers from two main limitations, namely, low (solar-to-chemical) energy conversion efficiency and low product selectivity. In addition, many systems, especially homogenous photocatalytic systems, use expensive sacrificial reagents. This section will focus on the low energy conversion efficiency and product selectivity in terms of their causes and optimization strategies, which are summarized in **Table 3.**

[H2] Low energy conversion efficiency

One of the main barriers of facilitating the industrial application of photocatalytic CO_2 reduction is its low energy conversion efficiency (below 1%), which has three main causes. Firstly, the utilization of solar energy is limited by the poor absorption of visible and IR lights by catalyst, parasitic light loss and light intensity gradient[7]. Secondly, CO_2 is difficult to be activated, owing to its stable linear symmetric structure with an average C=O bond energy up to 750 kJ mol^{-1}[17]. Thirdly, many of the proton-coupled electron transfers that are involved photocatalytic CO_2 conversion (as illustrated in **Fig. 5**) suffer from sluggish kinetics[15].

Energy conversion efficiency can be optimized from three aspects. The first one is exploiting catalysts with sufficient active sites, wide solar-spectrum absorption and efficient

charge separation. Defect engineering is an effective strategy that not only provides more sites for CO_2 adsorption but also enhances light harvesting while its effect on charge behaviours (namely, charge separation, migration, and recombination) is not unitary and requires elaborate control[155,157,158,185]. Doping metals or non-metals is another strategy to tune electronic structures and optical properties of inorganic-semiconductor-based catalysts. Doping can introduce impurity levels, with the dopants playing an important role in supressing charge recombination[19,34,37,186]. In addition, loading cocatalysts such as metal nanoparticles onto semiconductors can extend charge lifetime and provide more active sites. The optical absorption of co-catalysts does not necessarily contribute to CO_2 reduction, which needs further clarification[19,32,71,90]. Moreover, structural and morphological control of catalysts allows adequate exposure of active sites with short charge transfer paths toward catalyst surface[20,36,38,42,69,137,187]. From this perspective, porous materials, low-dimensional materials and molecular catalysts are preferred. Enhancing the basicity of catalyst surface is also a promising strategy because CO_2 can perform as an electron acceptor to be activated when the electrophilic carbon atom interacts with Lewis basic sites[77,188]. The functions of a catalyst should be synchronized in time and space to have appropriate overall dynamics. Alternatively, combining multiple components as a composite catalyst may make it easier to meet the complicated requirements of efficient photocatalytic CO_2 reduction. Combining two or more semiconductors to form p-n junction or Z-scheme promotes separation of charge carriers[19-21]. In addition, the role of light harvesting can be separated from supplying catalytically active sites given efficient interfacial charge transfer[55]. Interestingly, biotic species such as bacteria can be coupled with abiotic ones with electrons and protons (or H_2) transferred across interface, boosting photocatalytic CO_2 reduction[88,90,91].

The second approach to enhance energy conversion efficiency is to optimize reactor and operation conditions. An ideal reactor should ensure efficient mass, photon, and heat transfers, which can be improved by adjusting its shape, size, and material[8,167]. The placement of solid catalyst, as a slurry, fixed bed, or film coated on a substrate, is another essential factor[17]. A rational design of substrates that allows sufficient exposure to light and reactants can significantly increase energy conversion efficiency for a wide range of catalysts[97,132,133]. Moreover, since different catalysts have different optimal reaction conditions to achieve their highest CO_2 reduction efficiency, selecting an appropriate reductant and solvent and tuning the feed ratio, pressure, catalyst dosage and reaction time show a great promise to further enhance energy conversion efficiency.

The development of thermo-photo synergetic catalytic processes has emerged as a promising approach to address the low efficiency of photocatalysis and reduce the large energy consumption of thermal catalysis[17,73,97,157,187]. Thermal energy is either *in-situ* generated via photo-thermal effect or supplied with external heat source, which promotes photocatalysis through enhancing the kinetic driving force of reactants, tuning redox

potentials, facilitating charge carrier migration, accelerating mass transfer, promoting reactant dissociation, and/or adjusting catalyst structure[17,73,97,177].

[H2] Low product selectivity

Low product selectivity is another major limitation of photocatalytic CO_2 reduction, which is caused by the complex multi-electron photoreduction reactions toward various carbon-containing substances and competitive H_2 evolution reaction in the presence of proton source. Low product selectivity imposes burdens on downstream utilization as separation and purification of products are required. The possible methods to address this issue are as follows.

First, the reaction pathway for every catalytic system should be clarified to determine the best route to direct the reaction toward the desirable product and terminate its further conversion[15,148]. In-depth understanding on reaction pathway at the molecular level can be developed via *in-situ* characterization techniques. However, the contribution of theoretical calculations to mechanistic understanding is limited because they cannot rigorously model real photocatalytic CO_2 reduction systems.

Product selectivity can be tuned by choosing catalysts with appropriate energy band positions. Only thermodynamically favoured CO_2 reduction reactions with redox potentials more positive than the CBM of the catalyst can proceed. Other effective strategies for selectivity control include adjusting energy band positions of a certain catalyst via doping[186,189,190], size tuning (inducing quantum size effect)[191] anddefect engineering[73,97].

Furthermore, orienting surface reactions is an important approach to regulate product selectivity, owing to the high dependency of product selectivity on the destiny of surface species, namely, either desorption or further conversion[17,192]. Surface reactions can be oriented by tuning the catalyst surface (for example, elaborately designing the surface structure of nanosized catalysts)[38,149,183] and the chemical structure of molecular catalysts[63,64]. In addition, cocatalyst loading[72], crystal facet engineering[137,193], surface layer coating[194], and particle size optimization[32] of solid catalysts might help to control product selectivity. Surface reactions can be oriented by adjusting reaction medium and condition. For example, if one product shows a high solubility in reaction medium under the operation condition, it can easily desorb from catalyst surface without further conversion to higher-reduction-state products, leading to its high selectivity. However, in a closed photocatalytic system, the continuous accumulation of a product might result in its further conversion or the backward reaction.

[H1] Outlook

Photocatalytic CO_2 reduction is a sustainable strategy that utilizes renewable solar energy to produce high-value chemicals and fuels. Photoelectrocatalytic CO_2 reduction has been widely studied since 1979[16,158,198-200], and excellent reviews have been provided[201,202]. The number of publications in this emerging field has dramatically increased over recent years and

is ever growing. Numerous inspiring progresses have been made in catalyst exploitation, reactor design, process optimization and mechanism exploration, leading to significant improvement of photocatalytic performance. Nevertheless, photocatalytic CO_2 reduction is still far from practical application mainly due to its uncompetitive activity and selectivity. Here eight directions for boosting the development of this promising field are outlined.

Firstly, existing information of the kinetics of various steps in a photocatalytic CO_2 reduction process, active sites and reaction intermediates is deficient, causing a black box of reaction mechanism. However, a thorough and deep mechanistic understanding is necessary for designing efficient catalysts and catalytic systems. To acquire solid information, *in-situ* irradiated characterizations at high spatial, temporal, and spectral resolutions should be developed[137,140,141,144]. In addition, several papers claimed that DFT calculations show or demonstrate their reaction mechanisms, which are not true. Current computational methods cannot rigorously model complex photocatalytic CO_2 reduction systems and energy surfaces in excited states. There is still a long way to go to find a reliable computational method to elucidate catalytic mechanisms. Otherwise, calculation results just serve as a supplementary reference of experimental results.

Secondly, catalyst design is the core of promoting photocatalytic performance. An ideal catalyst should demonstrate high efficiency, desirable selectivity, excellent stability/recyclability, low cost, and environmental friendliness. To optimize catalytic efficiency, wide solar-spectrum absorption, effective charge separation, and sufficient active sites must be ensured. To acquire desirable selectivity, the energy band positions and surface structure of catalysts should be elaborately designed. To achieve excellent stability/recyclability, the catalyst should have a good resistance to photo-corrosion and all involved chemical substances including reactants, intermediates, and products. The economic viability and environmental impacts should be comprehensively evaluated via systematic techno-economic analysis and life cycle assessment. More strategies of optimizing catalysts can be developed on top of present defect engineering, doping, cocatalyst modification, size regulation, structural and morphological control, surface basicity enhancement, and heterostructure fabrication. Porous materials, low-dimensional materials and molecular catalysts show great promise to realize high photocatalytic performance for CO_2 reduction, owing to efficient mass and charge transfers and their regulatable structures. In addition, the application of biological species such as bacteria and enzymes in photocatalytic CO_2 reduction that exhibit great product selectivities[84-86,88,90,91,100] deserves more research attentions.

Following the last perspective on experimental exploration of efficient catalysts, advanced first-principles computation and machine learning techniques can assist the screening of candidate materials for photocatalytic CO_2 reduction, owing to recent advances in available computational power and computational methods[154,195]. For example, 52 materials stood out from 68,860 candidates after screening with their synthesizability, visible-light

absorption, compatibility of the electronic structure with CO_2 reduction, and corrosion resistance[195]. Nevertheless, a large computational dataset of material properties is required for facilitating further applications of data-driven techniques. The utilization of big data and machine learning augmented by robotic automation based on existing knowledge of CO_2 photocatalysis[7,196] may pave the way for photocatalyst development.

Despite wide investigation of heterogenous photocatalytic CO_2 reduction processes, studies in homogenous photocatalytic CO_2 reduction are still in infancy. The use of molecular catalysts in homogenous photocatalytic CO_2 reduction is a promising approach because of the easy and ready fine-tuning of ligand structures via controlling steric and electronic effects and their adequate exposure to CO_2, which may lead to highly efficient and selective processes[63,64,103,197]. Future research may be focused on the exploitation of cheap and earth-abundant metal complex catalysts, simplification or automation of catalyst synthesis procedure, improvement of other system components including photosensitizer, electron donor and solvent, and scale-up of current millilitre-level reactors.

Photocatalytic CO_2 reduction can be promoted by introducing another energy source such as thermal, electric, magnetic, ultrasonic, microwave,or mechanical energy, for efficient synergetic catalytic processes[17]. Among these synergetic processes, thermo-photo catalytic CO_2 reduction is the most attractive because thermal energy can be supplied by the photo-thermal effect. The photo-thermal effect can be locally induced by the catalyst itself[187,203,204] or globally with a solar furnace[182], eliminating the burden on energy consumption. Here, the thermal energy enhances the kinetic driving force of reactants[73,97]. Thermo-photo catalysis perfectly suits gas-phase reactions conducted in flow reactors such as CO_2 hydrogenation[73,157,187] and CO_2 reforming of CH_4[97,177,178] since parabolic trough solar concentrators are commercially available.

More effort should be made in the utilization of low-concentration CO_2 feedstock with potential interfering species, for practical application. Currently, 1 atm or even pressurized high-purity CO_2 is used as feedstock. To narrow the gap between laboratorial investigation and practical application, photocatalytic tests with CO_2 concentrations down to ppm level in the presence of other gases such as O_2, N_2, and SO_2, are expected. The entire catalytic system including catalyst, reductant, reactor and operation conditions should be optimized to attain satisfying performance of converting low-concentration CO_2 to desirable products.

Selective production of multi-carbon substances remains a great challenge. Most multi-carbon substances demonstrate higher market prices and more versatile uses than those of C1 chemicals (**Table 1**), which offers strong driving force for improving multi-carbon product selectivity. The complicated and sluggish kinetics of converting CO_2 to multi-carbon substances and the lack of catalytic activity toward C-C coupling are two main barriers[9,192,205]. It is believed that every factor that benefits the accumulation of charge carriers and protons, such as high photon flux and cocatalyst modification, favours the formation of multi-carbon products[9].

Furthermore, the catalyst should keep a balance between its abilities for hydrogenation and C-C coupling, which may reference to those applied in Fischer-Tropsch synthesis.

Finally, it is highly desirable to realize the transition from laboratory to practical and scalable applications in the next 10-20 years. This requires a large effort in catalyst optimization, modelling and construction of catalytic reactor and supporting facilities such as CO_2 collector, solar concentrator and product separator, assessment of economic and environmental benefits. Ultimately, photocatalytic CO_2 reduction will be an effective and sustainable answer to the critical issues related to energy and environment.

Photocatalytic CO_2 reduction is a highly promising method to valorize the anthropogenic CO_2 emissions, having raised a huge amount of research interests in the science community. A thorough understanding of this method, from the physical and chemical principles to the experimentation techniques and data reporting standards, is crucial for obtaining reliable and useful conclusions and driving the ongoing progress in our shared area. This Primer is expected to help overcome the current issues with data reproducibility and deposition and facilitate the laboratory-to-industry transition through combining the elaborate design of catalytic systems and deep exploration of reaction mechanisms. We believe that, with greater interactions and collaborations among experimental scientists, theorists, engineers, and regulatory agencies, more exciting discoveries are ahead.

Glossary

Thermal catalysis: The process of accelerating a chemical reaction with a catalyst and driven by thermal energy.

Heterogenous process: The process where the components are in multiple phases.

Homogenous process: The process where all components are in the same phase.

Semiconductor energy band gap: The energy difference between the valence band maximum and the conduction band minimum of a semiconductor.

Valence band maximum: The top of the highest range of electronic states which are occupied by electrons at absolute zero temperature.

Conduction band minimum: The bottom of the lowest range of vacant electronic states.

Localized surface plasmon resonance: The coherent collective oscillation of conduction band electrons in metal nanoparticles excited by the electromagnetic of incident light.

Hot charge carriers: The high-energy non-equilibrium electrons and holes resulting from the decay of plasmonic excitation.

Scherrer equation: The formula that relates the size of sub-micrometre crystallites in a solid to the broadening of a peak in an X-ray diffraction pattern.

De Broglie wavelength: The wavelength manifested in all objects in quantum mechanics which determines the probability density of finding the object at a given point of the configuration space.

Turnover number: The number of catalytic cycles (here, CO_2 molecules converted) per active site in a certain time.

Turnover frequency: The turnover number per unit time.

References

1 Wang, L. *et al.* Surface strategies for catalytic CO_2 reduction: from two-dimensional materials to nanoclusters to single atoms. *Chem. Soc. Rev.* **48**, 5310-5349 (2019). **This article summarizes the surface modification strategies for low-dimensional catalysts applied in heterogeneous photocatalytic CO_2 reduction.**

2 Friedlingstein, P. *et al.* Global carbon budget 2022. *Earth Syst. Sci. Data* **14**, 4811-4900 (2022).

3 Al-Ghussain, L. Global warming: review on driving forces and mitigation. *Environ. Prog. Sustainable Energy* **38**, 13-21 (2019).

4 Armstrong McKay, D. I. *et al.* Exceeding 1.5°C global warming could trigger multiple climate tipping points. *Science* **377**, eabn7950 (2022).

5 Li, X., Yu, J., Jaroniec, M. & Chen, X. Cocatalysts for selective photoreduction of CO_2 into solar fuels. *Chem. Rev.* **119**, 3962-4179 (2019). **This is a comprehensive review regarding the roles, designs, modifications, and applications of cocatalysts for photocatalytic CO_2 reduction.**

6 Kong, T., Jiang, Y. & Xiong, Y. Photocatalytic CO_2 conversion: what can we learn from conventional CO_x hydrogenation? *Chem. Soc. Rev.* **49**, 6579-6591 (2020).

7 Ozin, G. Accelerated optochemical engineering solutions to CO_2 photocatalysis for a sustainable future. *Matter* **5**, 2594-2614 (2022).

8 Tountas, A. A. *et al.* Towards solar methanol: past, present, and future. *Adv. Sci.* **6**, 1801903 (2019).

9 Albero, J., Peng, Y. & García, H. Photocatalytic CO_2 reduction to C2+ products. *ACS Catal.* **10**, 5734-5749 (2020).

10 Wei, J., Yao, R., Han, Y., Ge, Q. & Sun, J. Towards the development of the emerging process of CO_2 heterogenous hydrogenation into high-value unsaturated heavy hydrocarbons. *Chem. Soc. Rev.* **50**, 10764-10805 (2021).

11 Li, M., Sun, Z. & Hu, Y. H. Catalysts for CO_2 reforming of CH_4: a review. *J. Mater. Chem. A* **9**, 12495-12520 (2021).

12 Wagner, A., Sahm, C. D. & Reisner, E. Towards molecular understanding of local chemical environment effects in electro- and photocatalytic CO_2 reduction. *Nat. Catal.* **3**, 775-786 (2020).

13 Birdja, Y. Y. *et al.* Advances and challenges in understanding the electrocatalytic conversion of carbon dioxide to fuels. *Nat. Energy* **4**, 732-745 (2019).

14 Wang, C., Sun, Z., Zheng, Y. & Hu, Y. H. Recent progress in visible light photocatalytic conversion of carbon dioxide. *J. Mater. Chem. A* **7**, 865-887 (2019).

15 Chang, X., Wang, T. & Gong, J. CO_2 photo-reduction: insights into CO_2 activation and reaction on surfaces of photocatalysts. *Energy Environ. Sci.* **9**, 2177-2196 (2016).

16 Inoue, T., Fujishima, A., Konishi, S. & Honda, K. Photoelectrocatalytic reduction of

carbon dioxide in aqueous suspensions of semiconductor powders. *Nature* **277**, 637-638 (1979). **This is the first known report on heterogenous photocatalytic CO_2 reduction.**

17 Fang, S. & Hu, Y. H. Thermo-photo catalysis: a whole greater than the sum of its parts. *Chem. Soc. Rev.* **51**, 3609-3647 (2022).

18 Li, K., Peng, B. & Peng, T. Recent advances in heterogeneous photocatalytic CO_2 conversion to solar fuels. *ACS Catal.* **6**, 7485-7527 (2016).

19 Wang, Q. *et al.* Molecularly engineered photocatalyst sheet for scalable solar formate production from carbon dioxide and water. *Nat. Energy* **5**, 703-710 (2020). **This is a representative work of heterogenizing a molecular catalyst on a light-absorbing semiconductor sheet.**

20 Wang, S. *et al.* Porous hypercrosslinked polymer-TiO_2-graphene composite photocatalysts for visible-light-driven CO_2 conversion. *Nat. Comm.* **10**, 676 (2019).

21 Wang, Y. *et al.* Direct and indirect Z-scheme heterostructure-coupled photosystem enabling cooperation of CO_2 reduction and H_2O oxidation. *Nat. Comm.* **11**, 3043 (2020).

22 Yan, T. *et al.* How to make an efficient gas-phase heterogeneous CO_2 hydrogenation photocatalyst. *Energy Environ. Sci.* **13**, 3054-3063 (2020).

23 Shangguan, W. *et al.* Molecular-level insight into photocatalytic CO_2 reduction with H_2O over Au nanoparticles by interband transitions. *Nat. Comm.* **13**, 3894 (2022).

24 Li, Y. *et al.* Boosting thermo-photocatalytic CO_2 conversion activity by using photosynthesis-inspired electron-proton-transfer mediators. *Nat. Comm.* **12**, 123 (2021).

25 Zhang, X. *et al.* Product selectivity in plasmonic photocatalysis for carbon dioxide hydrogenation. *Nat. Comm.* **8**, 14542 (2017).

26 Devasia, D., Wilson, A. J., Heo, J., Mohan, V. & Jain, P. K. A rich catalog of C–C bonded species formed in CO_2 reduction on a plasmonic photocatalyst. *Nat. Comm.* **12**, 2612 (2021).

27 Zhan, C. *et al.* Plasmon-mediated chemical reactions. *Nat. Rev. Methods Primers* **3**, 12 (2023).

28 Zhan, C. *et al.* Disentangling charge carrier from photothermal effects in plasmonic metal nanostructures. *Nat. Comm.* **10**, 2671 (2019).

29 Kuramochi, Y., Ishitani, O. & Ishida, H. Reaction mechanisms of catalytic photochemical CO_2 reduction using Re(I) and Ru(II) complexes. *Coord. Chem. Rev.* **373**, 333-356 (2018).

30 Yamazaki, Y., Takeda, H. & Ishitani, O. Photocatalytic reduction of CO_2 using metal complexes. *J. Photochem. Photobiol., C* **25**, 106-137 (2015). **This article provides an overview on homogenous photocatalytic CO_2 reduction processes over metal complexes.**

31 Perazio, A., Lowe, G., Gobetto, R., Bonin, J. & Robert, M. Light-driven catalytic

conversion of CO_2 with heterogenized molecular catalysts based on fourth period transition metals. *Coord. Chem. Rev.* **443**, 214018 (2021).

32 Dong, C. *et al.* Size-dependent activity and selectivity of carbon dioxide photocatalytic reduction over platinum nanoparticles. *Nat. Comm.* **9**, 1252 (2018).

33 Wan, L. *et al.* Cu_2O nanocubes with mixed oxidation-state facets for (photo)catalytic hydrogenation of carbon dioxide. *Nat. Catal.* **2**, 889-898 (2019).

34 Sayed, M. *et al.* Sustained CO_2-photoreduction activity and high selectivity over Mn, C-codoped ZnO core-triple shell hollow spheres. *Nat. Comm.* **12**, 4936 (2021).

35 Yan, T. *et al.* Polymorph selection towards photocatalytic gaseous CO_2 hydrogenation. *Nat. Comm.* **10**, 2521 (2019).

36 Li, H., Cheng, C., Yang, Z. & Wei, J. Encapsulated CdSe/CdS nanorods in double-shelled porous nanocomposites for efficient photocatalytic CO_2 reduction. *Nat. Comm.* **13**, 6466 (2022).

37 Shown, I. *et al.* Carbon-doped SnS_2 nanostructure as a high-efficiency solar fuel catalyst under visible light. *Nat. Comm.* **9**, 169 (2018).

38 Li, X. *et al.* Selective visible-light-driven photocatalytic CO_2 reduction to CH_4 mediated by atomically thin $CuIn_5S_8$ layers. *Nat. Energy* **4**, 690-699 (2019). **This work explores a representative 2D defect-rich photocatalyst for photocatalytic CO_2 reduction.**

39 Kuehnel, M. F., Orchard, K. L., Dalle, K. E. & Reisner, E. Selective photocatalytic CO_2 reduction in water through anchoring of a molecular Ni catalyst on CdS nanocrystals. *J. Am. Chem. Soc.* **139**, 7217-7223 (2017).

40 Feng, X. *et al.* Unlocking bimetallic active sites via a desalination strategy for photocatalytic reduction of atmospheric carbon dioxide. *Nat. Comm.* **13**, 2146 (2022).

41 Shi, Y. *et al.* Van der Waals gap-rich BiOCl atomic layers realizing efficient, pure-water CO_2-to-CO photocatalysis. *Nat. Comm.* **12**, 5923 (2021).

42 Di, J. *et al.* Isolated single atom cobalt in Bi_3O_4Br atomic layers to trigger efficient CO_2 photoreduction. *Nat. Comm.* **10**, 2840 (2019).

43 Chen, G. *et al.* Alumina-supported CoFe alloy catalysts derived from layered-double-hydroxide nanosheets for efficient photothermal CO_2 hydrogenation to hydrocarbons. *Adv. Mater.* **30**, 1704663 (2018).

44 Li, M. M. J. *et al.* CO_2 hydrogenation to methanol over catalysts derived from single cationic layer CuZnGa LDH precursors. *ACS Catal.* **8**, 4390-4401 (2018).

45 Huang, P. *et al.* Selective CO_2 reduction catalyzed by single cobalt sites on carbon nitride under visible-light irradiation. *J. Am. Chem. Soc.* **140**, 16042-16047 (2018).

46 Bie, C., Zhu, B., Xu, F., Zhang, L. & Yu, J. In situ grown monolayer N-doped graphene on CdS hollow spheres with seamless contact for photocatalytic CO_2 reduction. *Adv. Mater.* **31**, 1902868 (2019).

47 Zhu, X. *et al.* In-situ hydroxyl modification of monolayer black phosphorus for stable

photocatalytic carbon dioxide conversion. *Appl. Catal., B* **269**, 118760 (2020).

48 Zhao, F. *et al.* Two-dimensional gersiloxenes with tunable bandgap for photocatalytic H_2 evolution and CO_2 photoreduction to CO. *Nat. Comm.* **11**, 1443 (2020).

49 Roy, S. & Reisner, E. Visible-light-driven CO_2 reduction by mesoporous carbon nitride modified with polymeric cobalt phthalocyanine. *Angew. Chem. Int. Ed.* **58**, 12180-12184 (2019).

50 Wei, Y. *et al.* Highly efficient photocatalytic reduction of CO_2 to CO by in situ formation of a hybrid catalytic system based on molecular iron quaterpyridine covalently linked to carbon nitride. *Angew. Chem. Int. Ed.* **61**, e202116832 (2022).

51 Ma, B. *et al.* Hybridization of molecular and graphene materials for CO_2 photocatalytic reduction with selectivity control. *J. Am. Chem. Soc.* **143**, 8414-8425 (2021).

52 Sun, W. *et al.* Heterogeneous reduction of carbon dioxide by hydride-terminated silicon nanocrystals. *Nat. Comm.* **7**, 12553 (2016).

53 Hao, Y.-C. *et al.* Metal-organic framework membranes with single-atomic centers for photocatalytic CO_2 and O_2 reduction. *Nat. Comm.* **12**, 2682 (2021).

54 Niu, K. *et al.* A spongy nickel-organic CO_2 reduction photocatalyst for nearly 100% selective CO production. *Sci. Adv.* **3**, e1700921 (2017).

55 Jiang, Z. *et al.* Filling metal–organic framework mesopores with TiO_2 for CO_2 photoreduction. *Nature* **586**, 549-554 (2020). **This work develops an efficient heterostructure photocatalyst by growing the light-absorbing TiO_2 inside the catalytically active MOF backbone.**

56 Lan, G. *et al.* Biomimetic active sites on monolayered metal–organic frameworks for artificial photosynthesis. *Nat. Catal.* **5**, 1006-1018 (2022).

57 Zhou, J. *et al.* Linking oxidative and reductive clusters to prepare crystalline porous catalysts for photocatalytic CO_2 reduction with H_2O. *Nat. Comm.* **13**, 4681 (2022).

58 Zhong, W. *et al.* A covalent organic framework bearing single Ni sites as a synergistic photocatalyst for selective photoreduction of CO_2 to CO. *J. Am. Chem. Soc.* **141**, 7615-7621 (2019). **This report presents a covalent organic framework (COF) catalyst bearing single Ni sites for photocatalytic CO_2 reduction to CO.**

59 Stock, N. & Biswas, S. Synthesis of metal-organic frameworks (MOFs): routes to various MOF topologies, morphologies, and composites. *Chem. Rev.* **112**, 933-969 (2012).

60 Li, Y., Chen, W., Xing, G., Jiang, D. & Chen, L. New synthetic strategies toward covalent organic frameworks. *Chem. Soc. Rev.* **49**, 2852-2868 (2020).

61 Wang, J.-W. *et al.* Facile electron delivery from graphene template to ultrathin metal-organic layers for boosting CO_2 photoreduction. *Nat. Comm.* **12**, 813 (2021).

62 Yuan, H., Cheng, B., Lei, J., Jiang, L. & Han, Z. Promoting photocatalytic CO_2 reduction with a molecular copper purpurin chromophore. *Nat. Comm.* **12**, 1835 (2021).

63 Rao, H., Schmidt, L. C., Bonin, J. & Robert, M. Visible-light-driven methane formation

from CO_2 with a molecular iron catalyst. *Nature* **548**, 74-77 (2017). **This is a representative work on homogenous photocatalytic CO_2 reduction with a low-cost molecular iron catalyst.**

64 Guo, Z. *et al.* Selectivity control of CO versus $HCOO^-$ production in the visible-light-driven catalytic reduction of CO_2 with two cooperative metal sites. *Nat. Catal.* **2**, 801-808 (2019). **This work develops a binuclear molecular cobalt catalyst for homogenous photocatalytic CO_2 reduction toward formate.**

65 Wu, Y., Li, S., Chen, Y., He, W. & Guo, Z. Recent advances in noble metal complex based photodynamic therapy. *Chem. Sci.* **13**, 5085-5106 (2022).

66 Warnan, J. & Reisner, E. Synthetic organic design for solar fuel systems. *Angew. Chem. Int. Ed.* **59**, 17344-17354 (2020).

67 Hutton, G. A. M., Martindale, B. C. M. & Reisner, E. Carbon dots as photosensitisers for solar-driven catalysis. *Chem. Soc. Rev.* **46**, 6111-6123 (2017).

68 Lim, S. Y., Shen, W. & Gao, Z. Carbon quantum dots and their applications. *Chem. Soc. Rev.* **44**, 362-381 (2015).

69 Ma, Y. *et al.* Selective photocatalytic CO_2 reduction in aerobic environment by microporous Pd-porphyrin-based polymers coated hollow TiO_2. *Nat. Comm.* **13**, 1400 (2022).

70 Wang, S. *et al.* Intermolecular cascaded π-conjugation channels for electron delivery powering CO_2 photoreduction. *Nat. Comm.* **11**, 1149 (2020). **This work develops a photocatalyst consisting of conjugated polymers for photocatalytic CO_2 reduction to CO.**

71 Cao, Y. *et al.* Modulating electron density of vacancy site by single Au atom for effective CO_2 photoreduction. *Nat. Comm.* **12**, 1675 (2021).

72 Verma, P. *et al.* Charge-transfer regulated visible light driven photocatalytic H_2 production and CO_2 reduction in tetrathiafulvalene based coordination polymer gel. *Nat. Comm.* **12**, 7313 (2021).

73 Wang, C., Fang, S., Xie, S., Zheng, Y. & Hu, Y. H. Thermo-photo catalytic CO_2 hydrogenation over Ru/TiO_2. *J. Mater. Chem. A* **8**, 7390-7394 (2020).

74 Kang, Q. *et al.* Photocatalytic reduction of carbon dioxide by hydrous hydrazine over Au–Cu alloy nanoparticles supported on $SrTiO_3/TiO_2$ coaxial nanotube arrays. *Angew. Chem. Int. Ed.* **54**, 841-845 (2015).

75 Zhang, X. *et al.* Photocatalytic conversion of diluted CO_2 into light hydrocarbons using periodically modulated multiwalled nanotube arrays. *Angew. Chem. Int. Ed.* **51**, 12732-12735 (2012).

76 Jiang, M., Gao, Y., Wang, Z. & Ding, Z. Photocatalytic CO_2 reduction promoted by a $CuCo_2O_4$ cocatalyst with homogeneous and heterogeneous light harvesters. *Appl. Catal., B* **198**, 180-188 (2016).

77 Xie, S., Wang, Y., Zhang, Q., Deng, W. & Wang, Y. MgO- and Pt-promoted TiO_2 as an efficient photocatalyst for the preferential reduction of carbon dioxide in the presence of water. *ACS Catal.* **4**, 3644-3653 (2014). **This work compares the solid-vapor and solid-liquid-gas reaction modes for photocatalytic reduction of CO_2 with H_2O.**

78 Lu, K.-Q. *et al.* Rationally designed transition metal hydroxide nanosheet arrays on graphene for artificial CO_2 reduction. *Nat. Comm.* **11**, 5181 (2020).

79 Zhou, Y. *et al.* Regulating photocatalytic CO_2 reduction selectivity via steering cascade multi-step charge transfer pathways in 1 T/2H-WS_2/TiO_2 heterojuncitons. *Chem. Eng. J.* **447**, 137485 (2022).

80 Cao, S., Shen, B., Tong, T., Fu, J. & Yu, J. 2D/2D heterojunction of ultrathin MXene/Bi_2WO_6 nanosheets for improved photocatalytic CO_2 reduction. *Adv. Funct. Mater.* **28**, 1800136 (2018).

81 Di, J. *et al.* Cobalt nitride as a novel cocatalyst to boost photocatalytic CO_2 reduction. *Nano Energy* **79**, 105429 (2021).

82 Tu, W. *et al.* An in situ simultaneous reduction-hydrolysis technique for fabrication of TiO_2-graphene 2D sandwich-like hybrid nanosheets: graphene-promoted selectivity of photocatalytic-driven hydrogenation and coupling of CO_2 into methane and ethane. *Adv. Funct. Mater.* **23**, 1743-1749 (2013).

83 Badiani, V. M. *et al.* Engineering electro- and photocatalytic carbon materials for CO_2 reduction by formate dehydrogenase. *J. Am. Chem. Soc.* **144**, 14207-14216 (2022).

84 Miller, M. *et al.* Interfacing formate dehydrogenase with metal oxides for the reversible electrocatalysis and solar-driven reduction of carbon dioxide. *Angew. Chem. Int. Ed.* **58**, 4601-4605 (2019).

85 Woolerton, T. W., Sheard, S., Pierce, E., Ragsdale, S. W. & Armstrong, F. A. CO_2 photoreduction at enzyme-modified metal oxide nanoparticles. *Energy Environ. Sci.* **4**, 2393-2399 (2011).

86 Liu, X. *et al.* A genetically encoded photosensitizer protein facilitates the rational design of a miniature photocatalytic CO_2-reducing enzyme. *Nat. Chem.* **10**, 1201-1206 (2018).

87 Kang, F. *et al.* Rational design of a miniature photocatalytic CO_2-reducing enzyme. *ACS Catal.* **11**, 5628-5635 (2021).

88 Wang, X. *et al.* Photocatalyst-mineralized biofilms as living bio-abiotic interfaces for single enzyme to whole-cell photocatalytic applications. *Sci. Adv.* **8**, eabm7665 (2022).

89 Ye, J. *et al.* Solar-driven methanogenesis with ultrahigh selectivity by turning down H_2 production at biotic-abiotic interface. *Nat. Comm.* **13**, 6612 (2022).

90 Wang, Q., Kalathil, S., Pornrungroj, C., Sahm, C. D. & Reisner, E. Bacteria–photocatalyst sheet for sustainable carbon dioxide utilization. *Nat. Catal.* **5**, 633-641 (2022).

91 Sakimoto, K. K., Wong, A. B. & Yang, P. Self-photosensitization of nonphotosynthetic

bacteria for solar-to-chemical production. *Science* **351**, 74-77 (2016). **This work develops a biological-inorganic hybrid with non-photosynthetic bacteria and light-absorbing CdS nanoparticles.**

92 Lam, E. & Reisner, E. A TiO_2-Co(terpyridine)$_2$ photocatalyst for the selective oxidation of cellulose to formate coupled to the reduction of CO_2 to syngas. *Angew. Chem. Int. Ed.* **60**, 23306-23312 (2021).

93 Bi, Q.-Q. *et al.* Selective photocatalytic CO_2 reduction in water by electrostatic assembly of CdS nanocrystals with a dinuclear cobalt catalyst. *ACS Catal.* **8**, 11815-11821 (2018).

94 Liu, L., Zhao, H., Andino, J. M. & Li, Y. Photocatalytic CO_2 reduction with H_2O on TiO_2 nanocrystals: comparison of anatase, rutile, and brookite polymorphs and exploration of surface chemistry. *ACS Catal.* **2**, 1817-1828 (2012).

95 Wang, K. *et al.* Unravelling the CC coupling in CO_2 photocatalytic reduction with H_2O on Au/TiO_{2-x}: combination of plasmonic excitation and oxygen vacancy. *Appl. Catal., B* **292**, 120147 (2021).

96 Ran, J., Jaroniec, M. & Qiao, S.-Z. Cocatalysts in semiconductor-based photocatalytic CO_2 reduction: achievements, challenges, and opportunities. *Adv. Mater.* **30**, 1704649 (2018).

97 Han, B., Wei, W., Chang, L., Cheng, P. & Hu, Y. H. Efficient visible light photocatalytic CO_2 reforming of CH_4. *ACS Catal.* **6**, 494-497 (2016). **This is the first known report on photocatalytic CO_2 reduction by CH_4 owing to the synergetic effects of photo and thermal energies.**

98 Kornienko, N., Zhang, J. Z., Sakimoto, K. K., Yang, P. & Reisner, E. Interfacing nature's catalytic machinery with synthetic materials for semi-artificial photosynthesis. *Nat. Nanotechnol.* **13**, 890-899 (2018).

99 Fang, X., Kalathil, S. & Reisner, E. Semi-biological approaches to solar-to-chemical conversion. *Chem. Soc. Rev.* **49**, 4926-4952 (2020).

100 Zhang, H. *et al.* Bacteria photosensitized by intracellular gold nanoclusters for solar fuel production. *Nat. Nanotechnol.* **13**, 900-905 (2018).

101 Dalle, K. E. *et al.* Electro- and solar-driven fuel synthesis with first row transition metal complexes. *Chem. Rev.* **119**, 2752-2875 (2019).

102 Guo, Z. *et al.* Highly efficient and selective photocatalytic CO_2 reduction by iron and cobalt quaterpyridine complexes. *J. Am. Chem. Soc.* **138**, 9413-9416 (2016).

103 Bonin, J., Robert, M. & Routier, M. Selective and efficient photocatalytic CO_2 reduction to CO using visible light and an iron-based homogeneous catalyst. *J. Am. Chem. Soc.* **136**, 16768-16771 (2014).

104 Cometto, C. *et al.* A carbon nitride/Fe quaterpyridine catalytic system for photostimulated CO_2-to-CO conversion with visible light. *J. Am. Chem. Soc.* **140**, 7437-

7440 (2018).

105 Cancelliere, A. M. *et al.* Efficient trinuclear Ru(ii)–Re(i) supramolecular photocatalysts for CO_2 reduction based on a new tris-chelating bridging ligand built around a central aromatic ring. *Chem. Sci.* **11**, 1556-1563 (2020).

106 Hargreaves, J. S. J. Some considerations related to the use of the Scherrer equation in powder X-ray diffraction as applied to heterogeneous catalysts. *Catal. Struct. React.* **2**, 33-37 (2016).

107 Inkson, B. J. in *Materials characterization using nondestructive evaluation (NDE) methods* (eds Gerhard Hübschen, Iris Altpeter, Ralf Tschuncky, & Hans-Georg Herrmann) 17-43 (Woodhead Publishing, 2016).

108 Carter, C. B. & Williams, D. B. *Transmission electron microscopy: diffraction, imaging, and spectrometry*. (Springer, 2016).

109 Fang, S. & Hu, Y. H. Open the door to the atomic world by single-molecule atomic force microscopy. *Matter* **4**, 1189-1223 (2021).

110 Zhang, L., Ran, J., Qiao, S.-Z. & Jaroniec, M. Characterization of semiconductor photocatalysts. *Chem. Soc. Rev.* **48**, 5184-5206 (2019).

111 Zhang, Y., Xia, B., Ran, J., Davey, K. & Qiao, S. Z. Atomic-level reactive sites for semiconductor-based photocatalytic CO_2 reduction. *Adv. Energy Mater.* **10**, 1903879 (2020).

112 Wertz, J. *Electron spin resonance: elementary theory and practical applications*. (Springer Science & Business Media, 2012).

113 Van der Heide, P. *X-ray photoelectron spectroscopy: an introduction to principles and practices*. (John Wiley & Sons, 2011).

114 de Groot, F. High-resolution X-ray emission and X-ray absorption spectroscopy. *Chem. Rev.* **101**, 1779-1808 (2001).

115 Lambert, J. B., Mazzola, E. P. & Ridge, C. D. *Nuclear magnetic resonance spectroscopy: an introduction to principles, applications, and experimental methods*. (John Wiley & Sons, 2019).

116 Larkin, P. *Infrared and Raman spectroscopy: principles and spectral interpretation*. (Elsevier, 2017).

117 Makuła, P., Pacia, M. & Macyk, W. How to correctly determine the band gap energy of modified semiconductor photocatalysts based on UV–vis spectra. *J. Phys. Chem. Lett.* **9**, 6814-6817 (2018).

118 Miao, T. J. & Tang, J. Characterization of charge carrier behavior in photocatalysis using transient absorption spectroscopy. *J. Chem. Phys.* **152**, 194201 (2020).

119 Wang, S. *et al.* Electrochemical impedance spectroscopy. *Nat. Rev. Methods Primers* **1**, 41 (2021).

120 Jones, W. E., Jr. & Fox, M. A. Determination of excited-state redox potentials by phase-

modulated voltammetry. *J. Phys. Chem.* **98**, 5095-5099 (1994).

121 Zhang, Y., Petersen, J. L. & Milsmann, C. A luminescent zirconium(IV) complex as a molecular photosensitizer for visible light photoredox catalysis. *J. Am. Chem. Soc.* **138**, 13115-13118 (2016).

122 Kahn, A. Fermi level, work function and vacuum level. *Mater. Horiz.* **3**, 7-10 (2016).

123 Mohan, A. *et al.* Hybrid photo- and thermal catalyst system for continuous CO_2 reduction. *ACS Appl. Mater. Interfaces* **12**, 33613-33620 (2020).

124 Hurtado, L. *et al.* Solar CO_2 hydrogenation by photocatalytic foams. *Chem. Eng. J.* **435**, 134864 (2022).

125 Han, B. & Hu, Y. H. Highly efficient temperature-induced visible light photocatalytic hydrogen production from water. *J. Phys. Chem. C* **119**, 18927-18934 (2015).

126 Chen, S. *et al.* Thin-water-film-enhanced TiO_2-based catalyst for CO_2 hydrogenation to formic acid. *Chem. Commun.* **58**, 787-790 (2022).

127 Ola, O. & Maroto-Valer, M. M. Review of material design and reactor engineering on TiO_2 photocatalysis for CO_2 reduction. *J. Photochem. Photobiol., C* **24**, 16-42 (2015).

128 Gong, E. *et al.* Solar fuels: research and development strategies to accelerate photocatalytic CO_2 conversion into hydrocarbon fuels. *Energy Environ. Sci.* **15**, 880-937 (2022).

129 Tahir, M. & Amin, N. S. Photocatalytic CO_2 reduction with H_2O vapors using montmorillonite/TiO_2 supported microchannel monolith photoreactor. *Chem. Eng. J.* **230**, 314-327 (2013).

130 Wu, J. C. S., Lin, H.-M. & Lai, C.-L. Photo reduction of CO_2 to methanol using optical-fiber photoreactor. *Appl. Catal., A* **296**, 194-200 (2005).

131 Nguyen, T.-V. & Wu, J. C. S. Photoreduction of CO_2 in an optical-fiber photoreactor: effects of metals addition and catalyst carrier. *Appl. Catal., A* **335**, 112-120 (2008).

132 Liou, P.-Y. *et al.* Photocatalytic CO_2 reduction using an internally illuminated monolith photoreactor. *Energy Environ. Sci.* **4**, 1487-1494 (2011).

133 Xiong, Z. *et al.* Photocatalytic CO_2 reduction over V and W codoped TiO_2 catalyst in an internal-illuminated honeycomb photoreactor under simulated sunlight irradiation. *Appl. Catal., B* **219**, 412-424 (2017).

134 Chatterjee, T., Boutin, E. & Robert, M. Manifesto for the routine use of NMR for the liquid product analysis of aqueous CO_2 reduction: from comprehensive chemical shift data to formaldehyde quantification in water. *Dalton Trans.* **49**, 4257-4265 (2020).

135 Wang, L., Cheng, B., Zhang, L. & Yu, J. In situ irradiated XPS investigation on S-scheme TiO_2@$ZnIn_2S_4$ photocatalyst for efficient photocatalytic CO_2 reduction. *Small* **17**, 2103447 (2021).

136 Collado, L. *et al.* Unravelling the effect of charge dynamics at the plasmonic metal/semiconductor interface for CO_2 photoreduction. *Nat. Comm.* **9**, 4986 (2018).

137 Wu, Y. A. *et al.* Facet-dependent active sites of a single Cu_2O particle photocatalyst for CO_2 reduction to methanol. *Nat. Energy* **4**, 957-968 (2019). **This article offers atomic-level understanding of active sites and chemical reaction mechanisms via *in-situ* SFXM-ETEM technique.**

138 Yan, Z.-H. *et al.* Photo-generated dinuclear $\{Eu(II)\}_2$ active sites for selective CO_2 reduction in a photosensitizing metal-organic framework. *Nat. Comm.* **9**, 3353 (2018).

139 Wang, M. *et al.* CO_2 electrochemical catalytic reduction with a highly active cobalt phthalocyanine. *Nat. Comm.* **10**, 3602 (2019).

140 Abdellah, M. *et al.* Time-resolved IR spectroscopy reveals a mechanism with TiO_2 as a reversible electron acceptor in a TiO_2–Re catalyst system for CO_2 photoreduction. *J. Am. Chem. Soc.* **139**, 1226-1232 (2017).

141 Hu, Y. *et al.* Tracking mechanistic pathway of photocatalytic CO_2 reaction at Ni sites using operando, time-resolved spectroscopy. *J. Am. Chem. Soc.* **142**, 5618-5626 (2020).

142 Tan, T. H. *et al.* Unlocking the potential of the formate pathway in the photo-assisted Sabatier reaction. *Nat. Catal.* **3**, 1034-1043 (2020). **This article provides a mechanistic understanding on photo-activation of adsorbed formate intermediate in photocatalytic CO_2 hydrogenation.**

143 Dimitrijevic, N. M., Shkrob, I. A., Gosztola, D. J. & Rajh, T. Dynamics of interfacial charge transfer to formic acid, formaldehyde, and methanol on the surface of TiO_2 nanoparticles and its role in methane production. *J. Phys. Chem. C* **116**, 878-885 (2012).

144 Lee, J., Sorescu, D. C. & Deng, X. Electron-induced dissociation of CO_2 on TiO_2(110). *J. Am. Chem. Soc.* **133**, 10066-10069 (2011).

145 Verma, R. *et al.* Nickel-laden dendritic plasmonic colloidosomes of black gold: forced plasmon mediated photocatalytic CO_2 hydrogenation. *ACS Nano* **17**, 4526-4538 (2023).

146 Dhiman, M. *et al.* Plasmonic colloidosomes of black gold for solar energy harvesting and hotspots directed catalysis for CO_2 to fuel conversion. *Chem. Sci.* **10**, 6594-6603 (2019).

147 Qin, D. *et al.* Recent advances in two-dimensional nanomaterials for photocatalytic reduction of CO_2: insights into performance, theories and perspective. *J. Mater. Chem. A* **8**, 19156-19195 (2020).

148 Hussain, S., Wang, Y., Guo, L. & He, T. Theoretical insights into the mechanism of photocatalytic reduction of CO_2 over semiconductor catalysts. *J. Photochem. Photobiol., C* **52**, 100538 (2022).

149 Li, J. *et al.* Self-adaptive dual-metal-site pairs in metal-organic frameworks for selective CO_2 photoreduction to CH_4. *Nat. Catal.* **4**, 719-729 (2021). **This report presents the selective photocatalytic CO_2 reduction to CH_4 over the MOF incorporated with self-adaptive dual-metal-site pairs.**

150 Kovačič, Ž., Likozar, B. & Huš, M. Photocatalytic CO_2 reduction: a review of ab initio

mechanism, kinetics, and multiscale modeling simulations. *ACS Catal.* **10**, 14984-15007 (2020).

151 Chu, W., Zheng, Q., Prezhdo, O. V. & Zhao, J. CO_2 photoreduction on metal oxide surface is driven by transient capture of hot electrons: ab initio quantum dynamics simulation. *J. Am. Chem. Soc.* **142**, 3214-3221 (2020).

152 Mai, H., Le, T. C., Chen, D., Winkler, D. A. & Caruso, R. A. Machine learning for electrocatalyst and photocatalyst design and discovery. *Chem. Rev.* **122**, 13478-13515 (2022).

153 Cheng, S. *et al.* Emerging strategies for CO_2 photoreduction to CH_4: from experimental to data-driven design. *Adv. Energy Mater.* **12**, 2200389 (2022).

154 Zhu, Q., Gu, Y., Liang, X., Wang, X. & Ma, J. A machine learning model to predict CO_2 reduction reactivity and products transferred from metal-zeolites. *ACS Catal.* **12**, 12336-12348 (2022).

155 Gao, W. *et al.* Vacancy-defect modulated pathway of photoreduction of CO_2 on single atomically thin $AgInP_2S_6$ sheets into olefiant gas. *Nat. Comm.* **12**, 4747 (2021).

156 Andrei, V., Wang, Q., Uekert, T., Bhattacharjee, S. & Reisner, E. Solar panel technologies for light-to-chemical conversion. *Acc. Chem. Res.* **55**, 3376-3386 (2022).

157 Wang, L. *et al.* Black indium oxide a photothermal CO_2 hydrogenation catalyst. *Nat. Comm.* **11**, 2432 (2020).

158 Yu, H. *et al.* Synergy of ferroelectric polarization and oxygen vacancy to promote CO_2 photoreduction. *Nat. Comm.* **12**, 4594 (2021).

159 Wang, J.-W., Jiang, L., Huang, H.-H., Han, Z. & Ouyang, G. Rapid electron transfer via dynamic coordinative interaction boosts quantum efficiency for photocatalytic CO_2 reduction. *Nat. Comm.* **12**, 4276 (2021).

160 Baruch, M. F., Pander, J. E., III, White, J. L. & Bocarsly, A. B. Mechanistic insights into the reduction of CO_2 on tin electrodes using in situ ATR-IR spectroscopy. *ACS Catal.* **5**, 3148-3156 (2015).

161 Kortlever, R., Shen, J., Schouten, K. J. P., Calle-Vallejo, F. & Koper, M. T. M. Catalysts and reaction pathways for the electrochemical reduction of carbon dioxide. *J. Phys. Chem. Lett.* **6**, 4073-4082 (2015).

162 Wang, Y., Chen, E. & Tang, J. Insight on reaction pathways of photocatalytic CO_2 conversion. *ACS Catal.* **12**, 7300-7316 (2022).

163 Yamazaki, Y., Miyaji, M. & Ishitani, O. Utilization of low-concentration CO_2 with molecular catalysts assisted by CO_2-capturing ability of catalysts, additives, or reaction media. *J. Am. Chem. Soc.* **144**, 6640-6660 (2022).

164 Dong, Y. *et al.* Shining light on CO_2: from materials discovery to photocatalyst, photoreactor and process engineering. *Chem. Soc. Rev.* **49**, 5648-5663 (2020).

165 Schroeder, E. & Christopher, P. Chemical production using light: are sustainable

photons cheap enough? *ACS Energy Lett.* **7**, 880-884 (2022).

166 Loh, J. Y. Y., Kherani, N. P. & Ozin, G. A. Persistent CO_2 photocatalysis for solar fuels in the dark. *Nat. Sustain.* **4**, 466-473 (2021).

167 Van Gerven, T., Mul, G., Moulijn, J. & Stankiewicz, A. A review of intensification of photocatalytic processes. *Chem. Eng. Process.* **46**, 781-789 (2007).

168 Herron, J. A. & Maravelias, C. T. Assessment of solar-to-fuels strategies: photocatalysis and electrocatalytic reduction. *Energy Technol.* **4**, 1369-1391 (2016).

169 Xia, Y.-S. *et al.* Tandem utilization of CO_2 photoreduction products for the carbonylation of aryl iodides. *Nat. Comm.* **13**, 2964 (2022).

170 Song, L. *et al.* Visible-light photocatalytic di- and hydro-carboxylation of unactivated alkenes with CO_2. *Nat. Catal.* **5**, 832-838 (2022).

171 Ulmer, U. *et al.* Fundamentals and applications of photocatalytic CO_2 methanation. *Nat. Comm.* **10**, 3169 (2019).

172 Tavasoli, A. V., Preston, M. & Ozin, G. Photocatalytic dry reforming: what is it good for? *Energy Environ. Sci.* **14**, 3098-3109 (2021).

173 von der Assen, N., Voll, P., Peters, M. & Bardow, A. Life cycle assessment of CO_2 capture and utilization: a tutorial review. *Chem. Soc. Rev.* **43**, 7982-7994 (2014).

174 Trudewind, C. A., Schreiber, A. & Haumann, D. Photocatalytic methanol and methane production using captured CO_2 from coal-fired power plants. Part I – a life cycle assessment. *J. Clean. Prod.* **70**, 27-37 (2014).

175 Lewis, N. S. Developing a scalable artificial photosynthesis technology through nanomaterials by design. *Nat. Nanotechnol.* **11**, 1010-1019 (2016).

176 Faunce, T. *et al.* Artificial photosynthesis as a frontier technology for energy sustainability. *Energy Environ. Sci.* **6**, 1074-1076 (2013).

177 Li, M., Sun, Z. & Hu, Y. H. Thermo-photo coupled catalytic CO_2 reforming of methane: a review. *Chem. Eng. J.* **428**, 131222 (2022).

178 Shoji, S. *et al.* Photocatalytic uphill conversion of natural gas beyond the limitation of thermal reaction systems. *Nat. Catal.* **3**, 148-153 (2020).

179 Ye, R.-P. *et al.* CO_2 hydrogenation to high-value products via heterogeneous catalysis. *Nat. Comm.* **10**, 5698 (2019).

180 Wu, X. *et al.* Photocatalytic CO_2 conversion of $M_{0.33}WO_3$ directly from the air with high selectivity: insight into full spectrum-induced reaction mechanism. *J. Am. Chem. Soc.* **141**, 5267-5274 (2019).

181 Wang, L. *et al.* Bismuth vacancy-induced efficient CO_2 photoreduction in BiOCl directly from natural air: a progressive step toward photosynthesis in nature. *Nano Lett.* **21**, 10260-10266 (2021). **This work uses natural air as CO_2 feedstock, which is an important practice toward applications.**

182 Schäppi, R. *et al.* Drop-in fuels from sunlight and air. *Nature* **601**, 63-68 (2022).

183 Li, Z. *et al.* Engineered disorder in CO_2 photocatalysis. *Nat. Comm.* **13**, 7205 (2022).

184 Zhang, Y. *et al.* Photocatalytic CO_2 reduction: identification and elimination of false-positive results. *ACS Energy Lett.* **7**, 1611-1617 (2022).

185 Zhao, Y. *et al.* Defect-rich ultrathin ZnAl-layered double hydroxide nanosheets for efficient photoreduction of CO_2 to CO with water. *Adv. Mater.* **27**, 7824-7831 (2015).

186 Yan, T. *et al.* Bismuth atom tailoring of indium oxide surface frustrated Lewis pairs boosts heterogeneous CO_2 photocatalytic hydrogenation. *Nat. Comm.* **11**, 6095 (2020).

187 Cai, M. *et al.* Greenhouse-inspired supra-photothermal CO_2 catalysis. *Nat. Energy* **6**, 807-814 (2021). **This work develops a core@shell structured photocatalyst with strong photo-thermal effect for CO_2 hydrogenation.**

188 Xie, S. *et al.* Photocatalytic reduction of CO_2 with H_2O: significant enhancement of the activity of Pt–TiO_2 in CH_4 formation by addition of MgO. *Chem. Commun.* **49**, 2451-2453 (2013).

189 Wang, T. *et al.* In situ synthesis of ordered mesoporous Co-doped TiO_2 and its enhanced photocatalytic activity and selectivity for the reduction of CO_2. *J. Mater. Chem. A* **3**, 9491-9501 (2015).

190 Xing, M. *et al.* Modulation of the reduction potential of TiO_{2-x} by fluorination for efficient and selective CH_4 generation from CO_2 photoreduction. *Nano Lett.* **18**, 3384-3390 (2018).

191 Niu, P., Yang, Y., Yu, J. C., Liu, G. & Cheng, H.-M. Switching the selectivity of the photoreduction reaction of carbon dioxide by controlling the band structure of a g-C_3N_4 photocatalyst. *Chem. Commun.* **50**, 10837-10840 (2014).

192 Fu, J., Jiang, K., Qiu, X., Yu, J. & Liu, M. Product selectivity of photocatalytic CO_2 reduction reactions. *Mater. Today* **32**, 222-243 (2020).

193 Bai, S. *et al.* Two-dimensional g-C_3N_4: an ideal platform for examining facet selectivity of metal co-catalysts in photocatalysis. *Chem. Commun.* **50**, 6094-6097 (2014).

194 Zhang, H. *et al.* Surface-plasmon-enhanced photodriven CO_2 reduction catalyzed by metal-organic-framework-derived iron nanoparticles encapsulated by ultrathin carbon layers. *Adv. Mater.* **28**, 3703-3710 (2016).

195 Singh, A. K., Montoya, J. H., Gregoire, J. M. & Persson, K. A. Robust and synthesizable photocatalysts for CO_2 reduction: a data-driven materials discovery. *Nat. Comm.* **10**, 443 (2019). **This is the first report on applying first-principles computation to screen the robust and synthesizable photocatalysts for CO_2 reduction.**

196 Stach, E. *et al.* Autonomous experimentation systems for materials development: a community perspective. *Matter* **4**, 2702-2726 (2021).

197 Rao, H., Lim, C.-H., Bonin, J., Miyake, G. M. & Robert, M. Visible-light-driven conversion of CO_2 to CH_4 with an organic sensitizer and an iron porphyrin catalyst. *J. Am. Chem. Soc.* **140**, 17830-17834 (2018).

198 Andrei, V. *et al.* Long-term solar water and CO_2 splitting with photoelectrochemical BiOI–$BiVO_4$ tandems. *Nat. Mater.* **21**, 864-868 (2022).

199 Bhattacharjee, S. *et al.* Photoelectrochemical CO_2-to-fuel conversion with simultaneous plastic reforming. *Nat. Synth.* **2**, 182-192 (2023).

200 Pati, P. B. *et al.* Photocathode functionalized with a molecular cobalt catalyst for selective carbon dioxide reduction in water. *Nat. Comm.* **11**, 3499 (2020).

201 Tang, B. & Xiao, F.-X. An overview of solar-driven photoelectrochemical CO_2 conversion to chemical fuels. *ACS Catal.* **12**, 9023-9057 (2022).

202 Putri, L. K., Ng, B.-J., Ong, W.-J., Chai, S.-P. & Mohamed, A. R. Toward excellence in photocathode engineering for photoelectrochemical CO_2 reduction: design rationales and current progress. *Adv. Energy Mater.* **12**, 2201093 (2022).

203 Wang, S. *et al.* Grave-to-cradle upcycling of Ni from electroplating wastewater to photothermal CO_2 catalysis. *Nat. Comm.* **13**, 5305 (2022).

204 Xu, Y.-F. *et al.* High-performance light-driven heterogeneous CO_2 catalysis with near-unity selectivity on metal phosphides. *Nat. Comm.* **11**, 5149 (2020).

205 Yu, S., Wilson, A. J., Heo, J. & Jain, P. K. Plasmonic control of multi-electron transfer and C–C coupling in visible-light-driven CO_2 reduction on Au nanoparticles. *Nano Lett.* **18**, 2189-2194 (2018).

206 Sun, Z., Ma, T., Tao, H., Fan, Q. & Han, B. Fundamentals and challenges of electrochemical CO_2 reduction using two-dimensional materials. *Chem* **3**, 560-587 (2017).

207 Fang, S. & Hu, Y. H. Temperature, pressure, and adsorption-dependent redox potentials: I. processes of CO_2 reduction to value-added compounds. *Energy Sci. Eng.* **10**, 4520-4543 (2022).

208 Xu, F. *et al.* Unique S-scheme heterojunctions in self-assembled TiO_2/$CsPbBr_3$ hybrids for CO_2 photoreduction. *Nat. Comm.* **11**, 4613 (2020).

209 Bae, K.-L., Kim, J., Lim, C. K., Nam, K. M. & Song, H. Colloidal zinc oxide-copper(I) oxide nanocatalysts for selective aqueous photocatalytic carbon dioxide conversion into methane. *Nat. Comm.* **8**, 1156 (2017).

210 Liu, Y. *et al.* Phase-enabled metal-organic framework homojunction for highly selective CO_2 photoreduction. *Nat. Comm.* **12**, 1231 (2021).

211 Chen, X. *et al.* Bromo- and iodo-bridged building units in metal-organic frameworks for enhanced carrier transport and CO_2 photoreduction by water vapor. *Nat. Comm.* **13**, 4592 (2022).

Acknowledgements

Y.H.H. and S.F. acknowledge the support from National Science Foundation (CMMI-1661699). M.Rahaman. acknowledges the support from the European Commission with a Horizon 2020 Marie Skłodowska-Curie Individual European Fellowship (SolarFUEL, GAN 839763). E. R. acknowledges the support for a European Research Council (ERC) Consolidator Grant (MatEnSAP, no. 682833). M.Robert. acknowledges the Institut Universitaire de France (IUF) for partial financial support.

Author contributions

Introduction (S.F., J.B., E.R., M.Robert, G.A.O. and Y.H.H.); Experimentation (S.F., M.Rahaman, J.B., E.R., M.Robert, G.A.O. and Y.H.H.); Results (S.F., M.Rahaman, E.R., M.Robert, G.A.O. and Y.H.H.); Applications (S.F., E.R., M.Robert, G.A.O. and Y.H.H.); Reproducibility and data deposition (S.F., J.B., E.R., M.Robert, G.A.O. and Y.H.H.); Limitations and optimizations (S.F., E.R., M.Robert, G.A.O. and Y.H.H.); Outlook (S.F., E.R., M.Robert, G.A.O. and Y.H.H.); Overview of the Primer (S.F., M.Rahaman, J.B., E.R., M.Robert, G.A.O. and Y.H.H.).

Competing interests

The authors declare no competing interests.

Peer review information

Nature Reviews Methods Primers thanks [Referee#1 name] and the other, anonymous, reviewer(s) for their contribution to the peer review of this work.

Related links

U.S. Energy Information Administration: www.eia.gov

ChemAnalyst: www.chemanalyst.com

Tables

Table 1: Common products of photocatalytic CO_2 reduction.

Product	Half-reaction of CO_2 reduction	Redox potential (V)[a]	Annual production (10^9 kg)[b]	Market price (US \$ kg^{-1})[b]	Relevant uses[c]
CO	$CO_2 + 2e^- + 2H^+ \rightarrow CO + H_2O$	-0.52	32	0.1	Fischer-Tropsch synthesis, carbonylation of alkenes, metallurgy
$HCOO^-$	$CO_2 + 2e^- + H^+ \rightarrow HCOO^-$	-0.41	0.7	0.9	Preservative and antibacterial agent in livestock feed, leather and textile industry
HCHO	$CO_2 + 4e^- + 4H^+ \rightarrow HCHO + H_2O$	-0.48	23	0.4	Production of resins and polyfunctional alcohols, disinfection
CH_3OH	$CO_2 + 6e^- + 6H^+ \rightarrow CH_3OH + H_2O$	-0.38	85	0.6	Gasoline additive, fuel, production of HCHO, CH_3COOH and methyl tert-butyl ether
CH_4	$CO_2 + 8e^- + 8H^+ \rightarrow CH_4 + 2H_2O$	-0.24	2650	0.4	Fuel, reforming to syngas
$C_2O_4^{2-}$	$2CO_2 + 2e^- \rightarrow C_2O_4^{2-}$	-1.00	0.4	1.6	Cleaning, bleaching
CH_3COO^-	$2CO_2 + 8e^- + 7H^+ \rightarrow CH_3COO^- + 2H_2O$	-0.29	12	1.4	Solvent, food, production of vinyl acetate, acetic anhydride and ester
CH_3CHO	$2CO_2 + 10e^- + 10H^+ \rightarrow CH_3CHO + 3H_2O$	-0.36	1.0	2.0	Production of 2-ethyl-1-octanol and pentaerythritol
CH_3CH_2OH	$2CO_2 + 12e^- + 12H^+ \rightarrow CH_3CH_2OH + 3H_2O$	-0.33	81	1.1	Fuel, solvent, alcoholic beverage, antiseptic in medical uses
C_2H_4	$2CO_2 + 12e^- + 12H^+ \rightarrow C_2H_4 + 4H_2O$	-0.35	214	1.2	Production of ethylene oxide, ethylene dichloride, ethylbenzene and polyethylene
C_2H_6	$2CO_2 + 14e^- + 14H^+ \rightarrow C_2H_6 +$	-0.27	134	0.2	Production of C_2H_4,

	$4H_2O$				power generation, cryogenic refrigeration system

[a]The values of apparent standard redox potentials are relative to standard hydrogen electrode (SHE) at pH = 7[5,206,207].

[b]The annual productions and market prices in 2022 are mainly acquired from U.S. Energy Information Administration and ChemAnalyst .

[c]The relevant uses of CO_2 reduction products are referenced to [9]. The listed annual productions, market prices, and relevant uses of $HCOO^-$, $C_2O_4^{2-}$, and CH_3COO^- represent those of their conjugate acids, namely, HCOOH, $H_2C_2O_4$, and CH_3COOH, respectively.

Table 2: Data reporting required for photocatalytic CO_2 reduction.

Data	Definition and reporting requirement	Reporting format
Reporting of experimentation		
Chemicals and materials	Manufacturer, product number, and purity of all chemicals and materials	Description
Catalyst synthesis	Detailed step-by-step procedure of catalyst synthesis	Description
Catalyst characterization	Instrument model and test condition applied for catalyst characterizations	Description
Experimental setup	Scheme or photo of experimental setup with annotations on its dimensions and materials; Model, spectrum, and intensity of light source	Figure, description
Photocatalytic test	Detailed operation steps and conditions (pressure, feed ratio, catalyst dosage, *in-situ* probed temperature, and reaction time) of photocatalytic CO_2 reduction	Description
Product analysis	Apparatus (model, column, and detector), test condition (temperature, carrier gas/solvent, and flow rate), and calibration curve applied for product analysis	Description
Reporting of isotopic labelling results		
Isotopic labelling results	Photocatalytic test with $^{13}CO_2$ and subsequent product analysis via GC-MS and NMR with the spectra presented	Figure, description
Reporting of photocatalytic performance		
Production rate (all products)	Yield of a product per unit time per unit mass of catalyst	Numeric (μmol h^{-1} g^{-1})

Selectivity (all products)	Ratio of the yield of a product to the sum of the yields of all products	Numeric (%)
CO_2 conversion rate	Ratio of the amount of reacted CO_2 to the amount of supplied CO_2	Numeric (%)
Turnover frequency	Number of CO_2 molecules converted per active site per unit time	Numeric (h^{-1})
Apparent quantum efficiency (various wavelengths)	Ratio of the number of electrons participating in CO_2 reduction reactions to the number of incident photons	Numeric (%), figure
Solar-to-chemical efficiency	Ratio of the stored chemical energy to incident solar energy	Numeric (%)
Catalyst stability	Capability of the catalyst to maintain its activity in a long-term run	Figure
Catalyst recyclability	Capability of the catalyst to maintain its activity in multiple runs	Figure
Experimental uncertainty	Mean value and standard deviation calculated with more than 3 parallel catalytic tests	Error, error bar
Reporting of other essential data		
Catalyst information	Composition, structure, optical absorption, and energy band positions of catalyst; Characterizations of the spent catalyst if deactivation occurs in the long-term run	Figure, description
Photocatalytic mechanism	Experimental evidence and schemes of charge behaviours and reaction pathway	Figure, description
Negative controls	Tests in the absence of light irradiation, CO_2, reductant, catalyst, or solvent and subsequent product analysis	Numeric
Mass balance of carbon	Comparison of the amounts of carbon before and after photocatalytic tests	Numeric

Table 3: Limitations and optimizations of photocatalytic CO_2 reduction.

Limitation	Cause	Optimization
Low energy conversion efficiency	Limited utilization of solar energy; difficult activation of CO_2; sluggish kinetics of multiple proton-coupled electron transfers	Optimizing reactor and operation conditions; Developing thermo-photo catalytic processes; Exploiting catalysts with sufficient active sites, wide solar-spectrum absorption, and efficient charge separation via Introducing defects, Doping

		metals or non-metals, Loading cocatalysts, Tuning structure and morphology, Enhancing surface basicity, Combining multiple components (biotic and abiotic)
Low product selectivity	Complex multi-electron reduction reactions toward various carbon-containing products; Competitive H_2 evolution reaction	Clarifying reaction pathway; Choosing catalysts with appropriate energy band positions; Orienting surface reactions via tuning catalyst surface or adjusting reaction medium and condition

Box 1: Limitations and optimizations of photocatalytic CO_2 reduction

The two main limitations of photocatalytic CO_2 reduction are solar-to-chemical energy conversion efficiency and low product selectivity.

Low energy conversion efficiency

Causes:

- Limited utilization of solar energy
- Difficult activation of CO_2
- Sluggish kinetics of multiple proton-coupled electron transfers

Optimizations:

- Exploiting catalysts with sufficient active sites, wide solar-spectrum absorption, and efficient charge separation via:
  - Introducing defects
  - Doping metals or non-metals
  - Loading cocatalysts
  - Tuning structure and morphology
  - Enhancing surface basicity
  - Combining multiple components (biotic and abiotic)
- Optimizing reactor and operation conditions
- Developing thermo-photo catalytic processes

Low product selectivity

Causes:

- Complex multi-electron reduction reactions toward various carbon-containing products
- Competitive H_2 evolution reaction

Optimizations:

- Clarifying reaction pathway
- Choosing catalysts with appropriate energy band positions
- Orienting surface reactions via:
  - Tuning catalyst surface
  - adjusting reaction medium and condition

Figure legends

Fig. 1: Principles of photocatalytic CO_2 reduction. Heterogenous photocatalytic CO_2 reduction over **a**, single-semiconductor-based photocatalyst with cocatalyst (grey particle, which can be metals, carbon materials, metal complexes), **b**, p-n junction heterostructure photocatalyst, **c**, Z-scheme heterostructure photocatalyst, and **d**, metal-based photocatalyst with localized surface plasmon resonance effect. **e**, Homogeneous photocatalytic CO_2 reduction over molecular catalyst with photosensitizer.

Fig. 2: Flow chart of experimentation for photocatalytic CO_2 reduction. Step-by-step experimental procedure from catalyst synthesis and characterizations to reactor construction, photocatalytic test, and reaction mechanism exploration.

Fig. 3: Schematic reactors for photocatalytic CO_2 reduction. Batch reactors in **a**, solid-gas mode, **b**, solid-vapor mode, **c**, solid-liquid-gas mode, and **d**, liquid-gas mode. Flow reactors with catalysts coated on **e**, planar support, **f**, monolith support, and **g**, optical fibers.

Fig. 4: Literature overview of the numeric metrics in photocatalytic CO_2 reduction processes. a, Activity expressed as the logarithm of production rate per mass of catalyst. **b**, Selectivity among carbon-containing substances. **c**, CO_2 conversion rate (*vs.* pressure for batch reactors; *vs.* flow rate for flow reactors). **d**, Turnover number in the logarithm form. **e**, Apparent quantum efficiency. **f**, Solar-to-chemical efficiency. Metal-oxide-based catalysts (red symbols): Cu_2O-Pt/SiC/IrO_x[21]; Pt/SiO_2-TiO_2[32]; Pd/HPP-TiO_2[69]; $CsPbBr_3$/TiO_2[208]; Mn,C-ZnO[34]; Cu_2O-ZnO[209]; Cu_2O[137]; $In_2O_{3-x}(OH)_y$[35]; Bi_3TiNbO_9[158]. Other inorganic-semiconductor-based catalysts (orange symbols): Au/CdS[71]; C-SnS_2[37]; CotpyP/$SrTiO_3$:La,Rh|Au|RuO_2/$BiVO_4$:Mo[19]; Rh/$SrTiO_3$[178]; $CuIn_5S_8$[38]; $AgInP_2S_6$[155]; $Pb_{0.6}Bi_{1.4}O_2Cl_2$[40]; Gersiloxene[48]. Metal-based catalysts (yellow symbols): Au[23]; BiH_x[24]; SiH_x[52]. MOF/COF-based catalysts (green symbols): Ni/MOF[54]; Co/MOF[210]; Ir/MOF[53]; Ru/MOF[211]; Cu-Ni/MOF[149]; MOF-COF[57]; TiO_2/MOF[55]; CdSe/CdS-COF[36]; $Ru(phen)_3$/Eu-MOF[138]; Metalorganiczyme (monolayered MOF-based artificial enzyme)[56]. Molecular catalysts (blue symbols): Zn-TPY-TTF[72]; Pt/Zn-TPY-TTF[72]; Cu-PP/Fe-TDHPP[62]; Ir-QPY/Co-Pc[159]; $Ru(phen)_3$/Co-QPY[64]; Fe-p-TMA[63]. Bacteria-based catalysts (cyan symbols): M.b-NiCu-CdS[89]; S.o/Cr_2O_3/$SrTiO_3$:La,Rh|RuO_2/$BiVO_4$:Mo[90]. Enzyme-based catalysts (purple symbols): PSP/TPY[86]; CdS/$CsgA_{A7}$-FDH[88].

Fig. 5: Possible routes of heterogenous photocatalytic CO_2 reduction reaction. a, Monodentate or bidentate intermediate route. **b**, Surface-bound bicarbonate intermediate route. **c**, $\bullet CO_2^-$ radical intermediate route with the following formaldehyde pathway and carbene pathway. **d**, Glyoxal intermediate route. The important intermediates are highlighted in yellow.

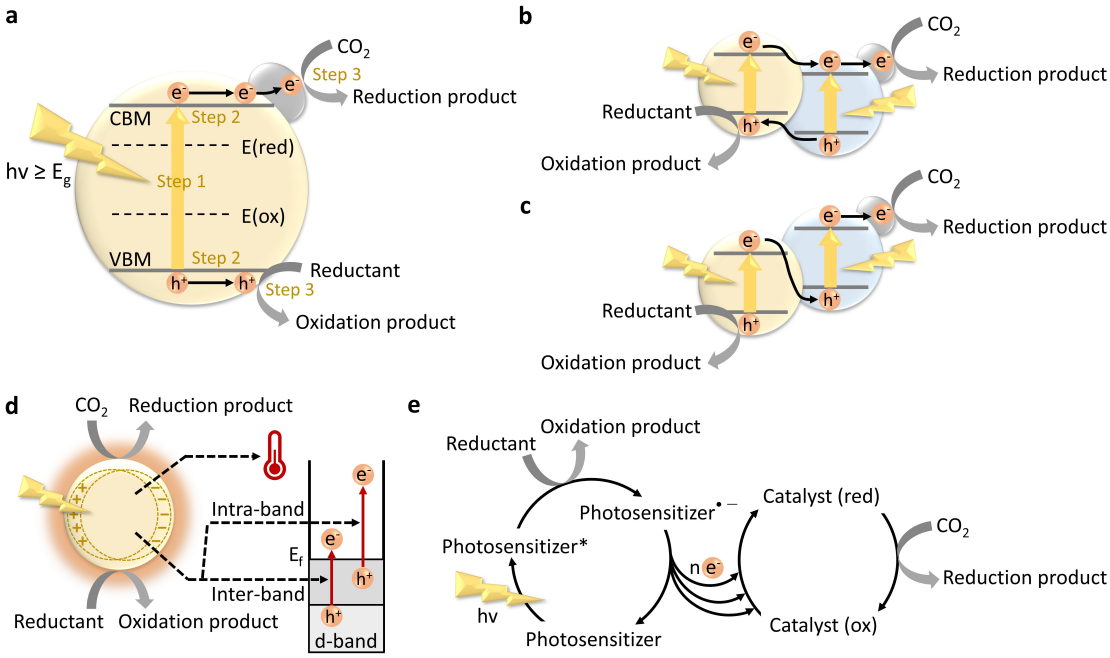

Flow Chart of Experimentation for Photocatalytic CO_2 Reduction

Step 1 – Synthesize catalyst
- Synthesize light absorber (or photosensitizer)
- Synthesize cocatalyst (or molecular catalyst)
- Assemble light absorber and cocatalyst

Step 2 – Characterize catalyst
- Structure (XRD, SEM, TEM, SPM, BET, EPR)
- Chemical state (XPS, XAS, NMR, FT-IR, Raman)
- Optical property (UV-vis, TAS, SPS, PL, i-t, EIS)
- Energy band position (M-S, XPS-VB, UV-vis)

Step 3 – Build photocatalytic reactor
- Batch reactor
- Flow reactor

Step 4 – Perform photocatalytic tests

(1) Operation condition
- Light source
- Reductant
- Pressure
- Reaction time
- Temperature
- Feed ratio
- Catalyst dosage
- Solvent (if any) and pH

(2) Measurement
- Product analysis (GC, NMR, LC, IC, GC-MS)
- Quantum/energy efficiency (Yield, light intensity, irradiation area)
- Catalyst stability/recyclability (Continuous test ≥ 50 hours or batch test ≥ 5 cycles)
- Isotopic labelling experiment (GC-MS, NMR)

Step 5 – Explore reaction mechanism
- *In-situ* or *ex-situ* experiment and characterization (XPS, XAS, EPR, SFXM, UV-vis, TAS, DRIFTS, STM)
- Theoretical calculation (First-principles calculation, machine learning)

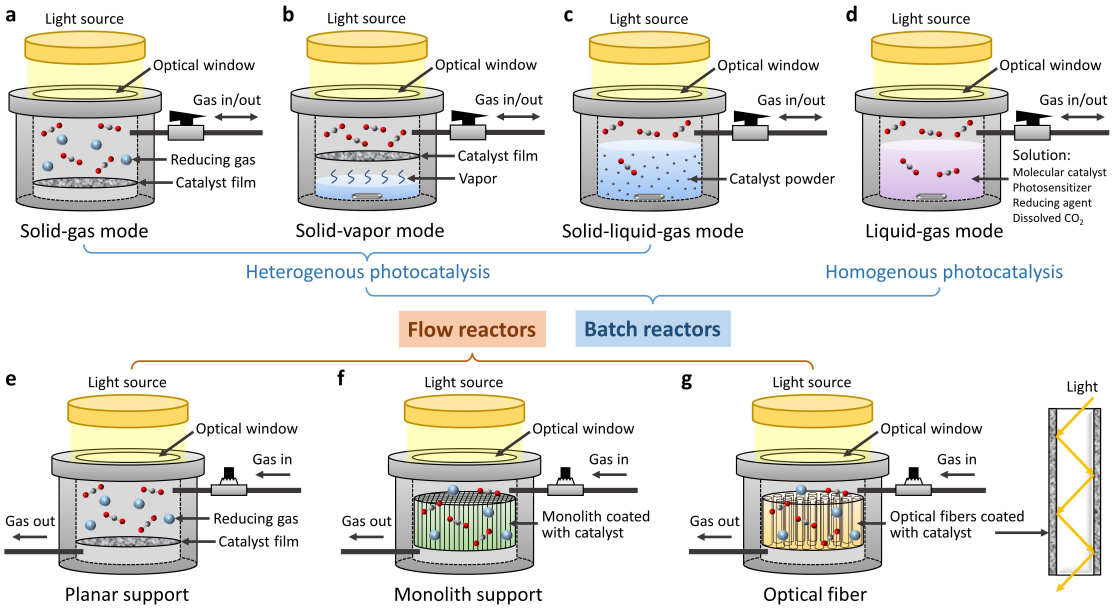
a
Light source
Optical window
Gas in/out
Reducing gas
Catalyst film
Solid-gas mode
b
Light source
Optical window
Gas in/out
Catalyst film
Vapor
Solid-vapor mode
c
Light source
Optical window
Gas in/out
Catalyst powder
Solid-liquid-gas mode
d
Light source
Optical window
Gas in/out
Solution:
Molecular catalyst
Photosensitizer
Reducing agent
Dissolved CO2
Liquid-gas mode
Heterogenous photocatalysis
Homogenous photocatalysis
Flow reactors
Batch reactors
e
Light source
Optical window
Gas in
Gas out
Reducing gas
Catalyst film
Planar support
f
Light source
Optical window
Gas in
Gas out
Monolith coated with catalyst
Monolith support
g
Light source
Optical window
Gas in
Gas out
Optical fibers coated with catalyst
Optical fiber
Light

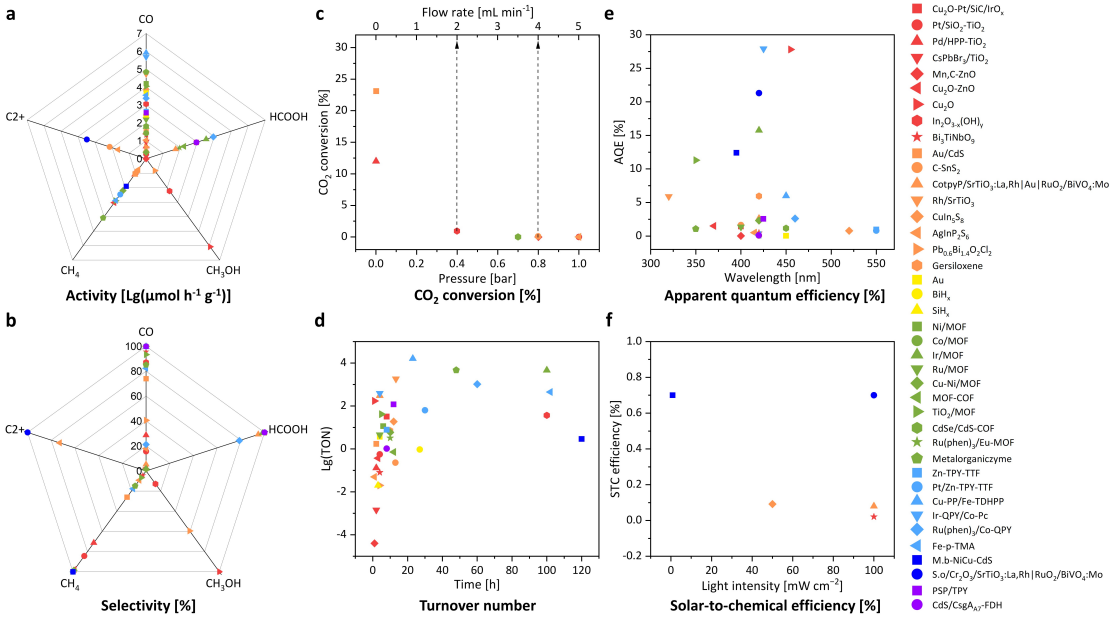
a
CO
HCOOH
C2+
CH4
CH3OH
Activity [Lg(μmol h-1 g-1)]
b
Selectivity [%]
c
Flow rate [mL min-1]
CO2 conversion [%]
Pressure [bar]
CO2 conversion [%]
d
Lg(TON)
Time [h]
Turnover number
e
AQE [%]
Wavelength [nm]
Apparent quantum efficiency [%]
f
STC efficiency [%]
Light intensity [mW cm-2]
Solar-to-chemical efficiency [%]
Cu2O-Pt/SiC/IrOx
Pt/SiO2-TiO2
Pd/HPP-TiO2
CsPbBr3/TiO2
Mn,C-ZnO
Cu2O-ZnO
Cu2O
In2O3-x(OH)y
Bi3TiNbO9
Au/CdS
C-SnS2
CotpyP/SrTiO3:La,Rh|Au|RuO2/BiVO4:Mo
Rh/SrTiO3
CuIn5S8
AgInP2S6
Pb0.6Bi1.4O2Cl2
Gersiloxene
Au
BiHx
SiHx
Ni/MOF
Co/MOF
Ir/MOF
Ru/MOF
Cu-Ni/MOF
MOF-COF
TiO2/MOF
CdSe/CdS-COF
Ru(phen)3/Eu-MOF
Metalorganiczyme
Zn-TPY-TTF
Pt/Zn-TPY-TTF
Cu-PP/Fe-TDHPP
Ir-QPY/Co-Pc
Ru(phen)3/Co-QPY
Fe-p-TMA
M,b-NiCu-CdS
S.o/Cr2O3/SrTiO3:La,Rh|RuO2/BiVO4:Mo
PSP/TPY
CdS/CsgAx,y-FDH

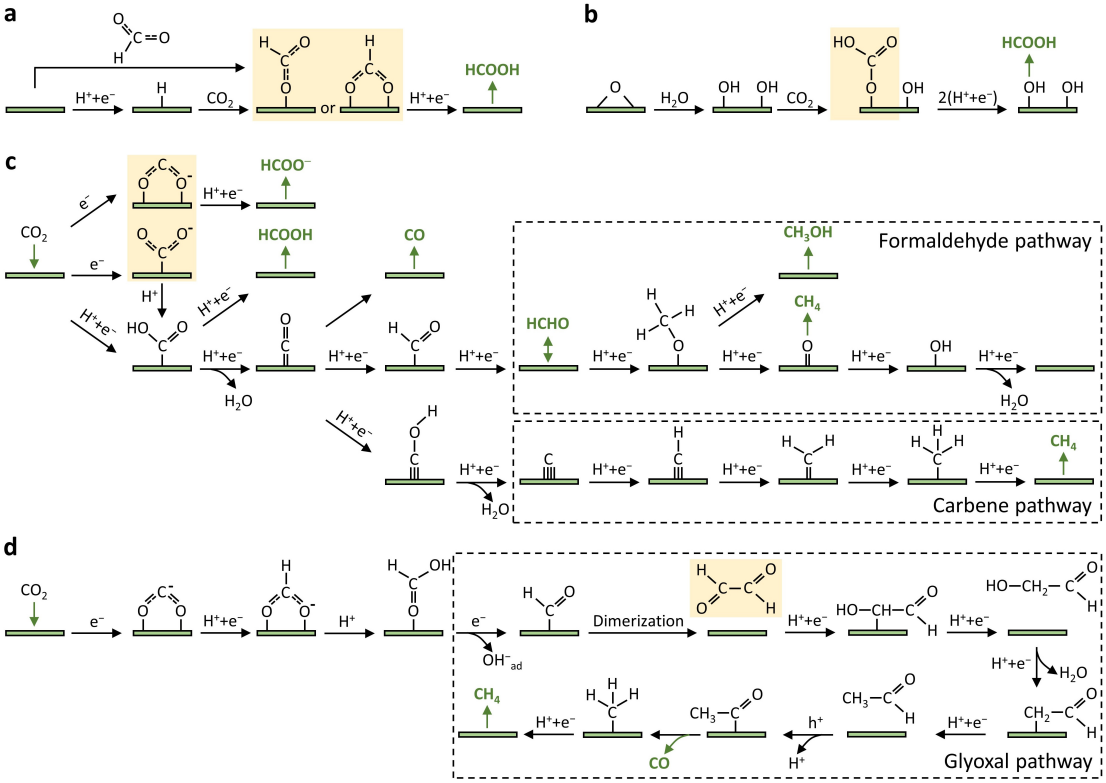
a
b
c
d
HCOOH
HCOO⁻
CO
CH₃OH
CH₄
HCHO
Formaldehyde pathway
Carbene pathway
Glyoxal pathway
Dimerization
2(H⁺+e⁻)